

Interference Cancellation in HSDPA Terminals

April 1, 2009

Contents

- 0.1 Introduction 1
- 0.2 UMTS Downlink and HSDPA 3
 - 0.2.1 Multiple Access in UMTS FDD Downlink 4
 - 0.2.2 UMTS Services 5
 - 0.2.3 HSDPA Features 6
 - 0.2.4 Downlink Transmission Model 10
- 0.3 Downlink Channel and HSDPA Signal Models 12
 - 0.3.1 Channel Impairments and Mitigation 12
 - 0.3.2 HSDPA Signal Model 17
- 0.4 Suppression of Intracell Interference in HSDPA 18
 - 0.4.1 Rake Receiver and LMMSE Chip Equalizer 18
 - 0.4.2 HSDPA Performance Analysis of Rake Receiver and Chip Equalizers 26
- 0.5 Advanced Receivers for Interference Cancellation 36
 - 0.5.1 Symbol-Rate Signal Model 36

0.5.2	Optimal Receiver	37
0.5.3	Decorrelating Receiver	37
0.5.4	LMMSE Receiver	42
0.5.5	Linear Parallel Interference Cancellation Receiver	43
0.5.6	Iterative Receivers based on Chip Equalizers	44

0.1 Introduction

Over-the-air communication is interference limited. Deployment of wireless networks therefore needs resource planning. Neighboring base stations in a cellular network could for instance transmit in different frequency bands. For such deployment, hexagonal cell geometry is assumed in cellular systems (see Figure 1) and resource planning is done by allocation of disjoint chunks of spectrum to neighboring base stations. The number of neighboring cells in which a certain frequency can be used only once is known in the cellular literature as *frequency reuse factor*. A frequency reuse factor of 7 results when isotropic antennas are deployed at cell-site (base station) and of 3 when using antenna sectorization of three sectors per hexagonal cell. Such frequency planning obviously aims interference avoidance, but it makes network deployment cumbersome and is wasteful of spectral resource. A direct sequence (DS)-CDMA system in principle boasts a frequency reuse factor of 1. In fact this factor was purportedly one of the main advantages of the first CDMA based cellular network, IS-95 [41]. Users can coexist in the same frequency spectrum. A resource is a spreading code and in the specific case of downlink communications, codes belong to a binary orthogonal set, the Walsh-Hadamard set. A base station has the entire set of codes at its disposal.

All base stations employ the same code-set as resources and each base station overlays a frame containing a number of spread symbols by a specific long pseudorandom code with quaternary alphabet called the scrambling code. The code helps the mobile station distinguish between base station signals.

Standard CDMA mobile receivers are matched-filters, matched to the spreading code of the signal (user) one needs to detect transmitted symbols of. When signal passes through a multipath channel, the receiver is matched to the cascade of the spreading code and the channel. The matched filter is also called *RAKE* receiver in the context of multipath signal due to one standard correlator-based implementation that resembles an agricultural rake, and where energy in delayed multipath signals are collected by correlating the delayed copies of the signal with the code of the user of interest.

User-specific spreading and base station-specific scrambling are the key elements of the

general structure of downlink communications in early-day CDMA systems like IS-95 and even circuit-switched UMTS [4] both of which supported low-rate applications. In the latter, maximum service data-rates of 384 kbps per base station using all physical channels resources are achievable while providing the necessary quality of service. Such rates are sufficient for applications like video-streaming.

Spreading and scrambling at the transmitter and corresponding descrambling and despreading at the receiver do not fundamentally change the communication paradigm but are simply elements of a multiple access method (CDMA). It is hoped that noise-like user signals rendered thus due to bandwidth expansion (spreading) will be rejected by the matched filter. All other transceiver stages such as error-control coding, interleaving to mitigate block-fading etc. are similar as in single-user communications.

A mobile station can be effected by two types of interference known in the literature as intracell and intercell interferences. In the particular case of downlink CDMA communications which we shall henceforth address, the former comes about due to multipath propagation in the channel. Indeed, the channel distorts signals in transit that were orthogonal upon transmission. The RAKE receiver is then limited in performance due to this interference sometimes also referred to as self-interference since even in the case of one transmitted code, copies of the signal interfere mutually. This is no different from the Inter-Symbol-Interference (ISI) problem in bandlimited channels. It was shown in [38], that the Signal-to-Interference-plus-Noise Ratio (SINR) of the RAKE receiver contains a per code interference term that is the sum of energies of all multipath components at the RAKE output scaled by the inverse of the spreading factor. As the number of codes increases for a given Spreading Factor (SF) as is the case in High-Speed Downlink Packet Access (HSDPA) where up to 15 codes with SF of 16 can coexist, the SINR at the RAKE output may degrade sufficiently to render communications impossible. Mitigation of intracell interference can be done through equalization-prior to despreading receivers [13].

In the downlink (HSDPA) context, intercell interference is the signal a mobile station sees from one or more neighboring base stations. Due to the propagation factors, the cell-boundary is not really a regular contour (e.g., a hexagon) and is only of figurative interest.

When frequency reuse is unity a good way of delimiting a cell is the strength of the signal. However, with full frequency reuse as in the case in CDMA, the Signal-to-Interference Ratio (SIR) experienced at the mobile station is a more appropriate cell-boundary notion. Users experience increasing levels of interference as they move from the base station/cell-site towards the cell-boundary. As interference could be a sum of interferences from several neighboring cell sites, it is customary [5] to define SIR as Signal to total-intercell-Interferences Ratio and each interfering-station to total-intercell-interference ratio is referred to as Dominant Interference Portion (DIP) ratio. Some reference numbers for these quantities are SIR of 0 dB with two interfering base stations with DIP of -2.75 and -7.64 dB respectively [5].

This chapter is organized as follows. Section 0.2 revisits the UMTS downlink signal and discusses HSDPA in relation with early-day non-packet UMTS. Section 0.3 describes the propagation environment and the channel model. Section 0.4 addresses the RAKE receiver, and some linear chip-level equalizers capable of dealing with intracell interference. Section 0.5 discusses intercell interference and presents a variety of solutions for suppression of this interference.

0.2 UMTS Downlink and HSDPA

We limit ourselves to the discussion of the UMTS WCDMA standard of which HSDPA is one component. This system is based on Frequency Division Duplexing (FDD) so that uplink and downlink transmissions occur in non-overlapping frequency bands. Thus a mobile terminal only sees signals from base stations. Another version of UMTS uses Time Division Duplexing (TDD) where mobile terminals could effectively see interference from terminals talking to other base stations unless strict time-scheduling rules are introduced. In spite of being an interesting problem in itself, UMTS TDD is beyond the scope of this discussion.

0.2.1 Multiple Access in UMTS FDD Downlink

In the UMTS downlink base stations transmit in frequency bands of 5MHz around the 2.1 GHz frequency. Each UMTS operator in general has two or three bands for the downlink transmission. The base station which is known as Node B in the UMTS radio access network (RAN) context is the source of transmissions for its *logical cell*. If a sectorized cell planning is deployed, then Node B is responsible for more than one logical cell as shown in Figure 1.

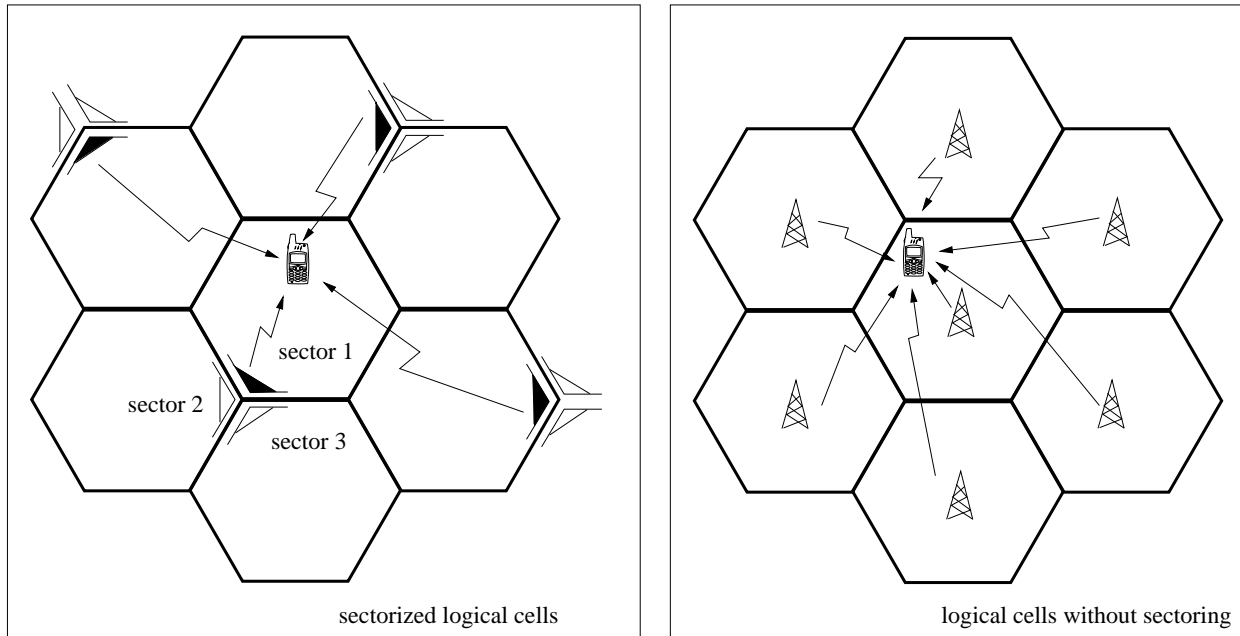


Figure 1: Logical cells differentiated by scrambling codes.

The signals transmitted from different logical cells are differentiated from each other by the assignment of different pseudo-random *scrambling* codes which are repeated every UMTS *frame* of 38400 chips, hence are known as *long* overlay codes.

Multi-access of the users in the same logical cell is realized by a CDMA scheme which uses *short* orthogonal *channelization* codes from various levels of the OVSF code tree shown in Figure 2 each level of which contains codes corresponding to the columns of the Walsh-Hadamard transformation (WHT) of relevant size. A channelization code assigned to a user is periodically used for the transmission of each symbol. Any particular code in the i -th position at the SF level t is related to its two closest child codes at SF level $t + 1$ with the

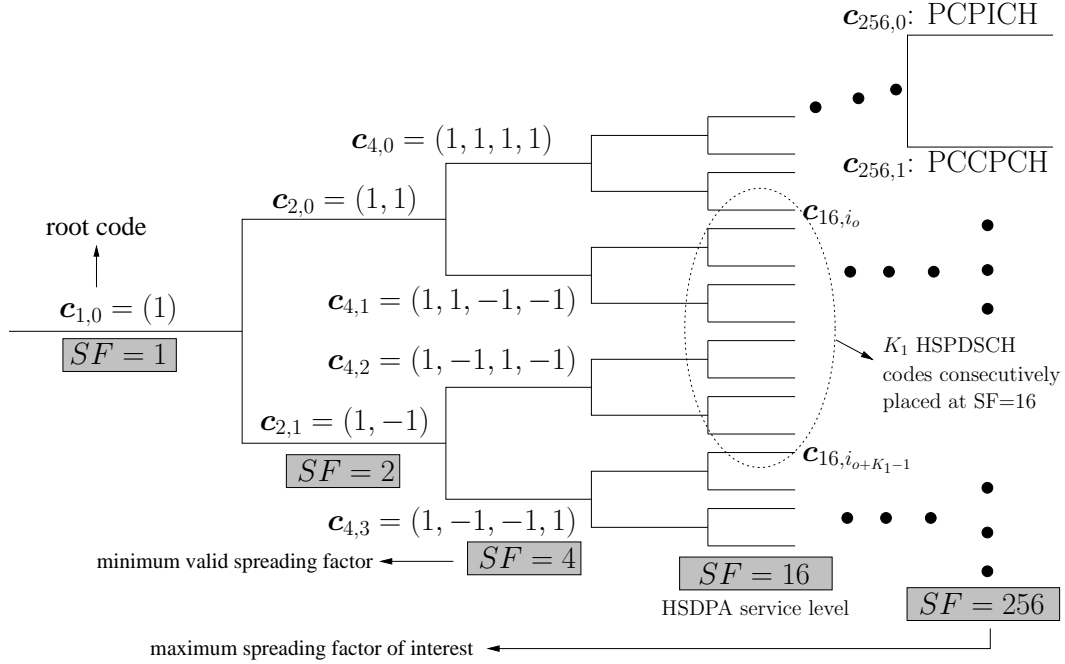


Figure 2: Partial schematic of the OVSF code tree.

transformation

$$\begin{bmatrix} \mathbf{c}_{2^{t+1}, 2^i} & \mathbf{c}_{2^{t+1}, 2^i+1} \end{bmatrix} = \begin{bmatrix} 1 & 1 \\ 1 & -1 \end{bmatrix} \otimes \mathbf{c}_{2^t, i} \quad (1)$$

where, \otimes stands for Kronecker product. The valid code lengths are from the set $\{2^t, t \in 2, 3, \dots, 9\}$. The largest code length, i.e., the spreading factor 512, is very rarely used. When a particular code is assigned to a user, then all its parent or child codes are blocked for usage in order to preserve orthogonality among used codes. These properties make UMTS FDD downlink a *code-limited* system. In case only a single spreading level is used from the OVSF tree, then the number of available codes for that particular scenario is upper-bounded by the associated spreading factor.

0.2.2 UMTS Services

The flexibility of using different length codes makes UMTS a *multi-rate* system, enabling services with different data-rates and thus different QoS.

Just like any other cellular multi-access system, a UMTS network must support a large number of users with different QoS and have ubiquitous coverage. Large coverage area of individual cells, i.e., decreasing the number of deployed base stations, decreases network user-capacity. On the other hand, more cells would mean more intercell interference. From this relation it is easy to see that in order to meet both coverage and user-capacity requirements, advanced transmission (diversity) or reception techniques are of use. The UMTS standard defines four QoS classes with differing delay and packet-ordering requirements [3]:

Conversational: low delay, strict ordering, e.g: voice

Streaming: modest delay, strict ordering, e.g: video

Interactive: modest delay, modest ordering, e.g: web browsing

Background: no delay guarantee, no ordering, e.g: bulk data transfer

0.2.3 HSDPA Features

Background and *Interactive* UMTS service classes have a burst nature enabling time-divided multiuser scheduling thus reaping the benefits of *multiuser diversity* [42]. This consideration triggered time-sharing system resources among users, most importantly the orthogonal codes in the downlink leading to the standardization of HSDPA in the UMTS Standard Release-5 [5].

Allocation of multiple access codes for HSDPA service: Motivated by the burst nature of the data, as shown in Figure 2, $K_1 \in \{1, 2, \dots, 15\}$ of the 16 channelization code resources at SF=16 are allocated as High Speed Physical Downlink Shared Channels (HSPDSCHs) and dynamically time multiplexed among demanding users in order to achieve a higher spectral efficiency and a larger link adaptation dynamic range. The variable $i_o \in \{1, 2, \dots, 15\}$ denotes the position of the first HSPDSCH code. The single *transport* channel counterpart spanning the HSPDSCHs of a user is called HSDSCH.

Fast scheduling of allocated codes: Multiuser diversity is obtained if there are independently varying temporal channel conditions for different users, leading to order increase

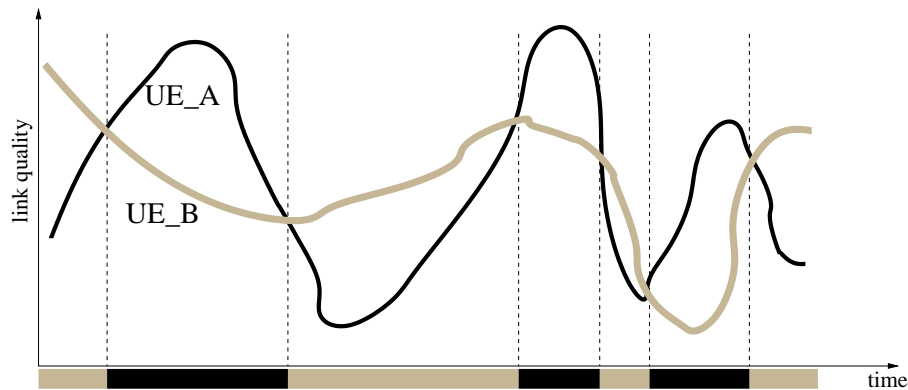


Figure 3: Principle of multiuser diversity.

in *sum capacity*, i.e., the total delivered payload by the BS. By one extreme approach, as demonstrated in Figure 3 in a simple 2-user system context, one can preferably assign all the codes to a single user with the instantaneously best channel conditions, maximizing the throughput. At the other extreme, users might be served in a *fair* round-robin fashion. In this respect operators are free to choose any set of schedulers compromising throughput and fairness by basing their decisions on the predicted channel quality, the cell load and the traffic priority class. In order to reduce the delay in signaling and to better track the channel variations, scheduling is performed at Node-B which is closer to the air interface compared to the Radio Network Controller (RNC) which was responsible with such tasks in the earlier standard releases. Moreover scheduling period is decreased to 2ms sub-frame duration, i.e., 1 TTI, from the 10ms frame duration of pre-HSDPA UMTS¹. Soft handover is also replaced by fast *best-signaling-cell* selection which can be considered as a kind of *spatial* scheduling complementing the *temporal* scheduling.

Link adaptation: As schematically demonstrated in Figure 4, perhaps one of the most important differences between HSDPA and its packet-switched ancestor (release 99 or R99 UMTS) is that there is *no fast power control* on HSPDSCHs and all the instantaneously remaining *allowed* BS power is assigned to HSPDSCHs which creates a high amount of power variation of HSPDSCH codes [2] over time. In this case, as can be interpreted from the figure, the system is also capable of utilizing the available BS power more

¹Low-end and medium-end HSDPA UEs which do not have enough buffering capability are obliged to wait at least two or three TTI periods respectively between two consecutive TTI data scheduling [5].

efficiently than the power controlled case. Furthermore, as shown in Figure 9, different user distances from the BS and different user mobility levels create a high amount of *inter-user link quality* differences. These two properties make Node-B scheduling more versatile in deciding for the number of allocated HSPDSCH codes, coding rate, puncturing rate and the modulation scheme, 16-QAM a possibility besides QPSK at high received power conditions, to maximize the throughput of the instantaneously scheduled user. For this purpose Node-B might use either the explicit CQI measurement reports from the UE based on the SINR of PCPICH or the known transmit power of the power-controlled downlink DPCH associated with the HSPDSCHs.

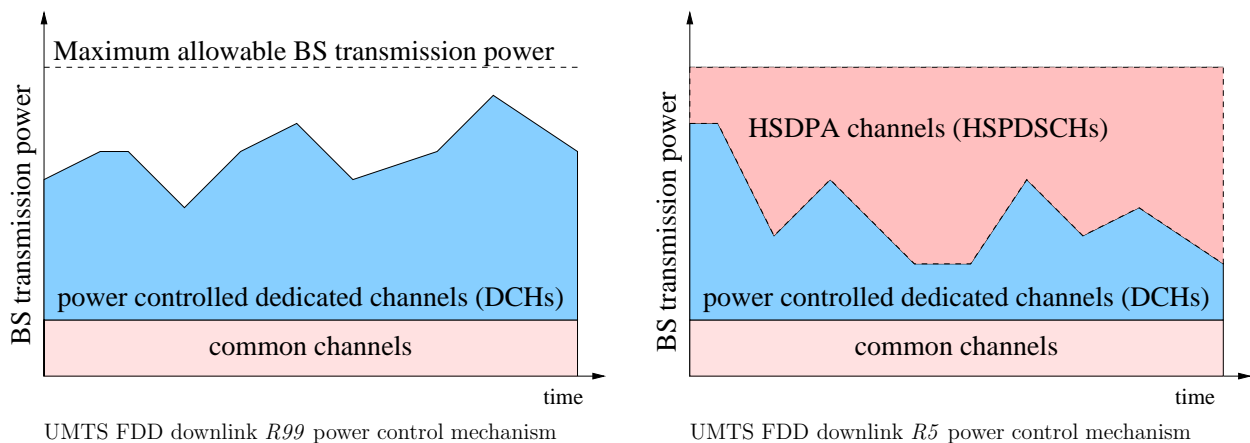


Figure 4: Power control with and without HSDPA.

Hybrid Automatic Repeat reQuest (HARQ): When transmission entities are identified to be erroneous by a standard protocol such as *selective-repeat* or *stop-and-wait*, fast retransmit request is done from Node-B and combinations of soft information from the original transmission and previous retransmissions are utilized to increase the probability of correct reception [19, 39]. These operations fine-tune the effective code rate, in a way compensating for errors in the channel quality estimates used for link adaptation. The two well known such methods are *chase combining* where weighting of identical retransmissions is done and the *incremental redundancy* where additional parity bits are sent each time.

To support the listed functionalities, two new channel types are introduced. In the downlink, one or more shared control channels (HSSCCHs) broadcast the scheduled UE identity,

the transport format and the HARQ process identifier. The UE monitors up to 4 different HSSCCHs and tries to find out if it is going to be scheduled or not. In the uplink, the High Speed Dedicated Physical Control Channel (HSDPCCH) carries the status reports for HARQ and the Channel Quality Indicators (CQIs). Figure 5 briefly demonstrates the order of events in the HSDPA transmission protocol. More detailed timing information and the slot structures are given in Figure 6 together with other UMTS channels relevant to the topics of the book chapter.

HSSCCH channel is frame aligned with the PCPICH channel which is in general used as a reference by several other UMTS channels and synchronization procedures as well.

HSPDSCHs are offset by 2 time slots w.r.t. HSSCCH which gives the UE some time to decode the time critical control and supervision information carried by the first slot of HSSCCH before receiving the HSDSCH payload data. Learning the scheduling of UE two slots beforehand is at the same time very useful for the *adaptive* equalizers that we will discuss in the following chapters. In order to do power savings, it is in general preferable to freeze the adaptation mechanism of an equalizer when the UE does not receive any HSDPA data. On the other hand it is beneficial to start the adaptation process some time earlier than the start of the useful data to force the equalizer to converge earlier.

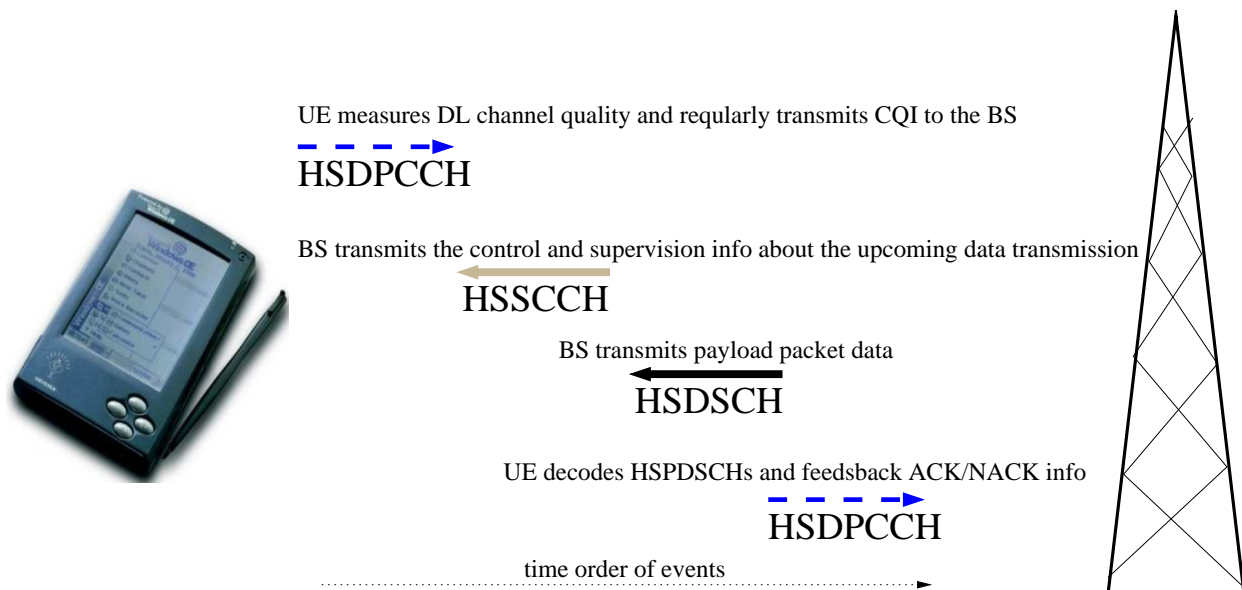


Figure 5: HSDPA transmission protocol.

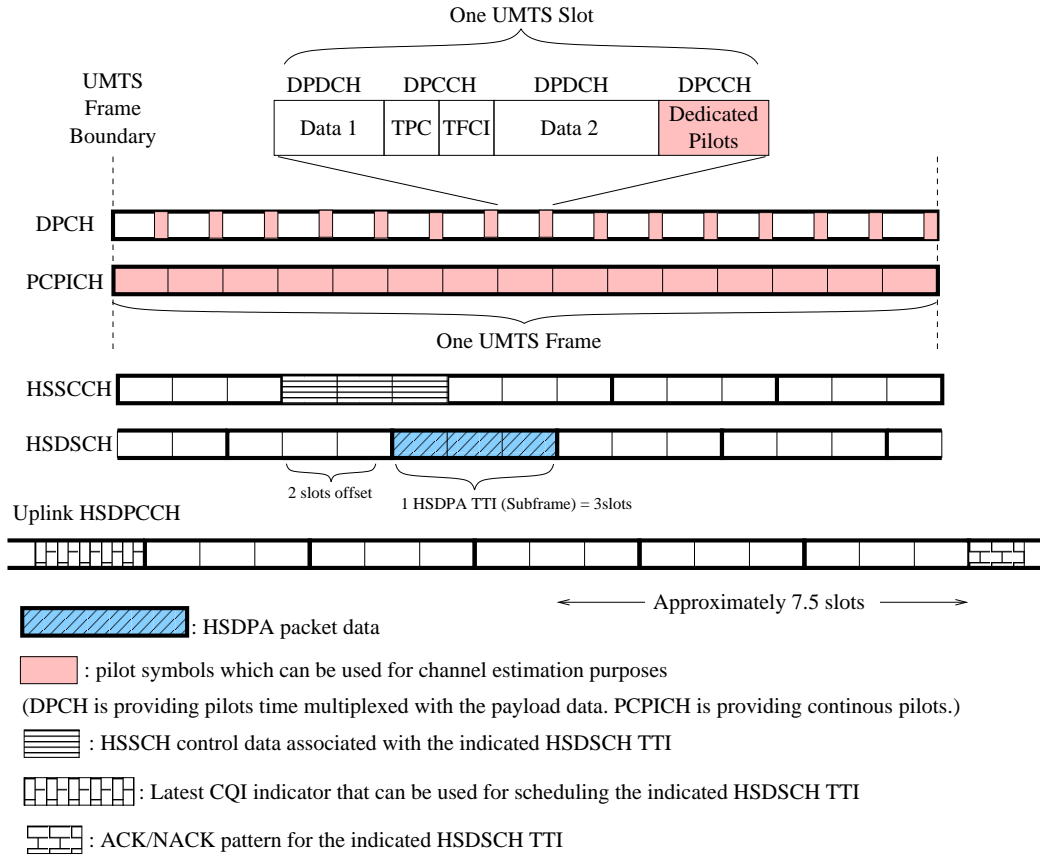


Figure 6: Slot structures and timings of UMTS channels of interest.

For a more detailed coverage of HSDPA, see [1, 6, 17, 12].

0.2.4 Downlink Transmission Model

The baseband downlink transmission model of the UMTS-FDD mode system with HSDPA support is given in Figure 7.

At the transmitter, the first group of K_1 i.i.d QPSK or 16-QAM modulated symbol sequences $\{a_1[n], a_2[n], \dots, a_{K_1}[n]\}$ which belong to the HSDPA transmission are first upsampled by a factor of 16 and then multiplied with their respective unit-amplitude channelization codes $\{\mathbf{c}_{16,i_o}, \mathbf{c}_{16,i_o+1}, \dots, \mathbf{c}_{16,i_o+K_1-1}\}$ shown in Figure 2. All HSPDSCH symbols have the same power and the same modulation scheme.

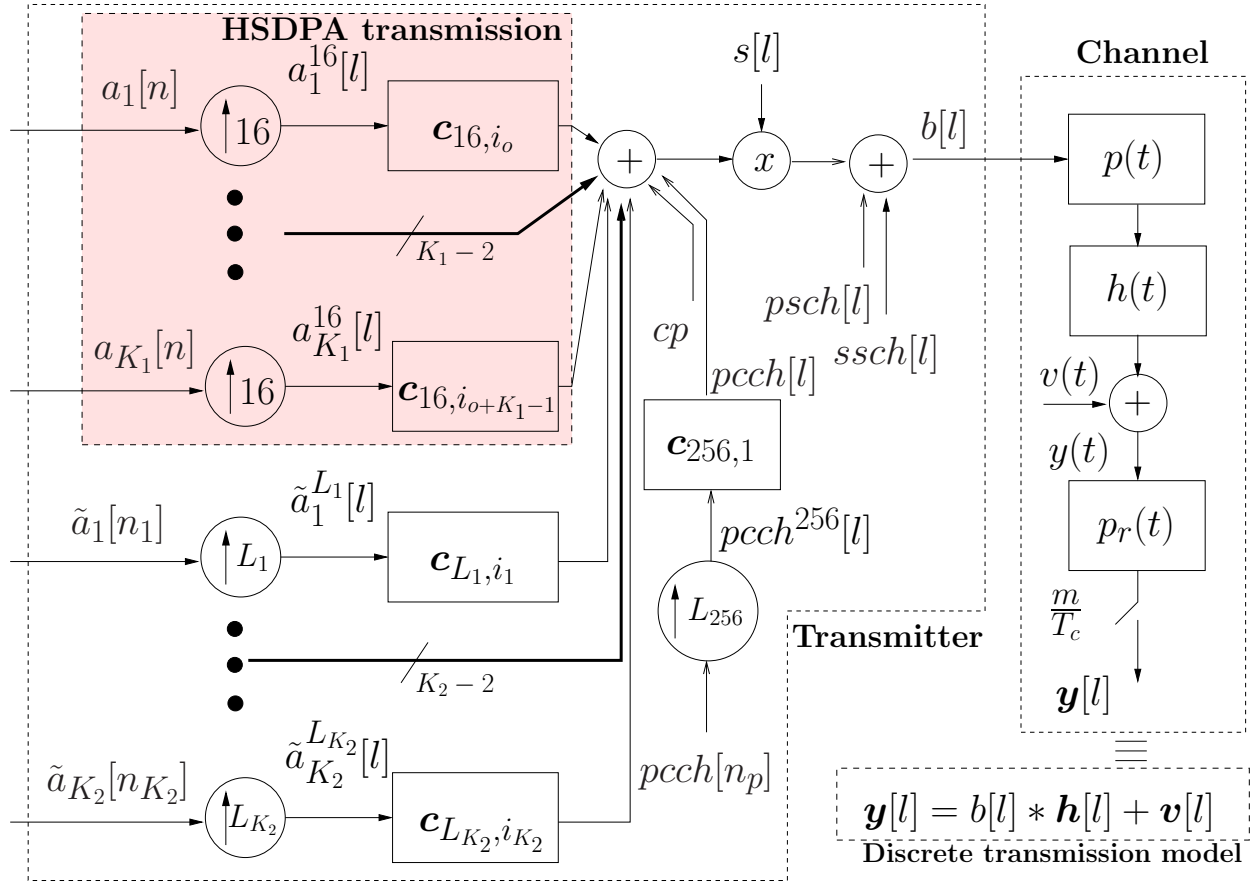


Figure 7: Baseband UMTS downlink transmission model.

The second group of multi-rate transmissions $\{\tilde{a}_1[n_1], \tilde{a}_2[n_2], \dots, \tilde{a}_{K_2}[n_{K_2}]\}^2$ representing the dedicated physical channels (DPCHs), HSSCCHs and other control channels are similarly upsampled and convolved with their respective channelization codes

$$\{\mathbf{c}_{L_1,i_1}, \mathbf{c}_{L_2,i_2}, \dots, \mathbf{c}_{L_{K_2},i_{K_2}}\}.$$

The third group of chip sequences associated with PCCPCH, PCPICH, PSCH and SSCH channels which are subjects to discussions in the following chapters are explicitly demonstrated as $pcch[l]$, cp , $psch[l]$ and $ssch[l]$ respectively. The common pilot, cp symbols are all $\frac{1+j}{\sqrt{2}}$.

The sum sequence of all the generated chip sequences is multiplied with the unit-energy BS-specific aperiodic scrambling sequence $s[l]$. PSCH and SSCH are the exceptions, mul-

²different symbol indices such as $n, n_1, n_2, \dots, n_{K_2}, n_p$ are used in the text and on Figure 7 to stress the *multi-rate* property of the transmission scheme

time-multiplexed after the scrambler, since as a first-step task in the receiver they are utilized for determining, i.e., searching, which scrambling sequence is assigned to the BS. The resultant effective BS chip sequence $b[l]$ is transmitted out on the channel.

0.3 Downlink Channel and HSDPA Signal Models

UMTS downlink channel has three cascade components in the order of a *root-raised-cosine* (rrc) pulse shape $p(t)$ with a roll-off factor of 0.22 shown in Figure 8, the *time-varying multipath propagation* channel $h(t)$ and a receiver front-end filter $p_r(t)$ which is in general chosen to be again an rrc pulse shape with a roll-off factor of 0.22 due to the fact that the *raised cosine* (rc) result of the rrc-rrc cascade is a *Nyquist pulse* whose T_c -spaced discrete time counterpart is a single unit pulse at time instant 0. In this case the only source of inter-chip interference (ICI) is $h(t)$. Alternatively a low pass antialiasing filter with a cutoff frequency between $\frac{1.22}{T_c}$ and $\frac{2}{T_c}$ might be considered as $p_r(t)$ in the case of twice chip rate sampling. The latter case is a reasonable choice for fractionally spaced equalizers [20, 21].

The *effective* continuous time channel is hence given as

$$h_{eff}(t) = p(t) * h(t) * p_r(t) \quad (2)$$

When there is no beamforming, the propagation channel and the effective overall channel are unique for all the transmitted data from the same BS.

0.3.1 Channel Impairments and Mitigation

Modeling of the propagation channel $h(t)$ is a very subtle and sophisticated field in itself [31, 32]. Therefore we restrict the discussion to intuitive explanations of some aspects which are essential for the book chapter.

The most observable effect of the propagation channel on the received signal quality is the time varying signal amplitude attenuation which is more often known as *fading* and is

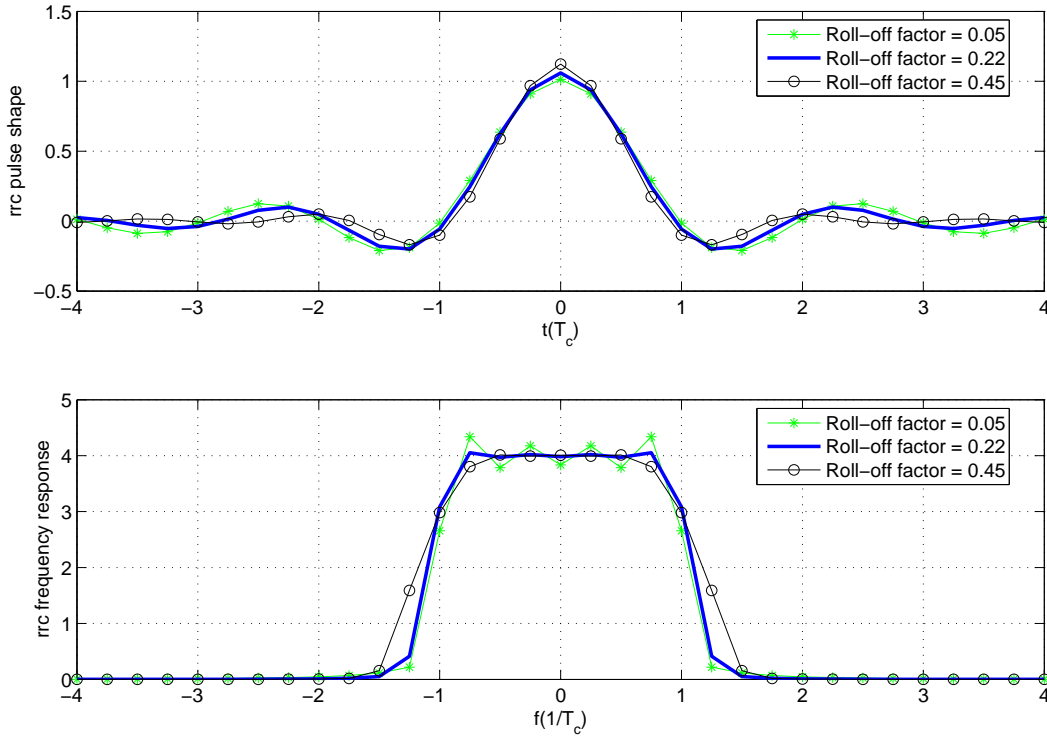


Figure 8: Root-raised cosine pulse shapes with different roll-off factors. Higher factors induce less ICI since the tails decay faster but they consume more bandwidth.

a combined consequence of different scale effects in space which however manifests itself in again different scales in time.

The environment-dependent *large-scale* statistics of the UE received power at a distance d in kilometers is modeled as³

$$P_r(\text{dBm}) = P_t(\text{dBm}) - G(\text{dB}) - 10n\log_{10}d(\text{dB}) + 10\log_{10}x(\text{dB}) \quad (3)$$

where P_t is the transmitted power⁴, G is the amount of path loss at a reference distance of 1km, n is the path loss exponent and x is the log-normal shadowing term with *geometric* mean 0 and *geometric* standard deviation σ_x . Shadowing is a consequence of signal absorption by the obstacles in the terrain between the BS and UE such as hills, trees, buildings, cars

³dBm is a relative measure w.r.t. 1mW power level

⁴In UMTS terminology $I_{or} = P_t$ and $\hat{I}_{or} = P_r$

and it causes a *variance* around the distance-dependent *mean* path loss. It is a *slow-fading* parameter which only varies when the UE changes its place by a distance proportional to the length of an obstructing object.

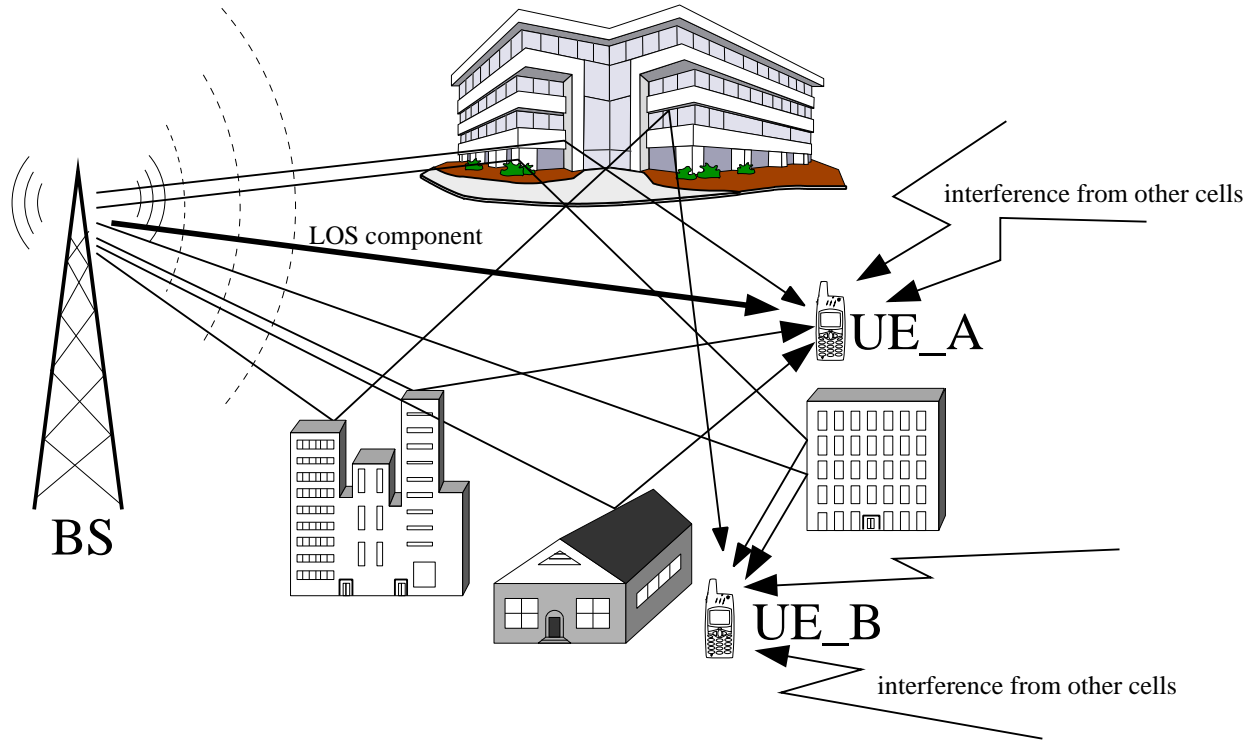


Figure 9: Multipath effect.

The most important propagation channel characteristics is the *multipath* effect. Infinitely many replicas of the transmitted signal which are reflected from several objects reach the UE with different delays and different complex attenuation factors. Specular replicas are clustered together to generate the effective multi-paths shown in Figure 9. The *sparse channel model* which takes into account only the most dominant P paths can be formulated as

$$h(t) = \sum_{i=1}^P h_i(t) \delta(t - \tau_i(t)) \quad (4)$$

The difference between the largest and smallest delay elements $\Delta_\tau = \tau_P - \tau_1$ is the *delay spread* of the channel. If $\Delta_\tau \geq T_c$, then the channel is *frequency selective*. This notion comes from the inverse of the delay spread known as *coherence bandwidth* $B_o \approx \frac{1}{\Delta_\tau}$. The physical meaning of B_o is that when two different sinusoidal components with frequencies f_1 and f_2 are

transmitted they are impacted differently by the channel if $\Delta f = |f_1 - f_2| \geq B_o$. In other words if the signal BW is larger than B_o , which is the case for UMTS *wideband* CDMA downlink, signal spectrum is non-uniformly affected by the channel. On one hand, if no channel equalization is applied this is a very dispersive situation driving the communication unreliable. On the other hand it is an opportunity to exploit the inherent *frequency diversity* coming from different sub-bands of the spectrum which are considered to be *independently fading*. In the time domain this property manifests itself in a different shape as the *resolution of the paths* which are separated from each other by at least a distance of T_c . Conventional Rake receiver exploits this fact by collecting energy via multiple correlations at time instants corresponding to the path delays. Although exact resolution is lower bounded by the chip period, some more diversity is expected from decreasing this constraint to slightly lower values such as $\frac{3T_c}{4}$ [8]. If an opposite situation occurs, i.e., if the signal BW is smaller than B_o , then the channel is *flat fading* meaning that there is no ICI. At first sight this seems to be a good situation not requiring a complicated equalization procedure. However when there are deep and long lasting channel fades as is the case in slow fading channels, other means such as transmit diversity or receive diversity are necessary to recover the UE from the *outage* state. These techniques, on the other hand, complicate the BS and the UE.

When all the specular components that generate one dominant path are modeled as *i.i.d.* complex random variables, by central limit theorem, channel parameters turn out to be circularly symmetric Gaussian random variables with zero mean and $2\sigma_i^2$ variance. Consequently, their complex envelope amplitudes are Rayleigh distributed.

$$p(|h_i(t)|) = \frac{|h_i(t)|}{\sigma_i^2} e^{-\frac{|h_i(t)|^2}{2\sigma_i^2}} \text{ for } |h_i(t)| \geq 0, \quad 0 \text{ otherwise} \quad (5)$$

When there is one very dominant line of sight (LOS) path as is the case for UE_A in Figure 9, its distribution is *Rician* which is more desirable since in that case there are less frequent and less deep fades. In this thesis we are not considering LOS situations.

Sparse multipath channel parameters are modeled to be wide sense stationary and uncorrelated with each other (WSS-US model) [31]. Therefore each one of them experiences an independent *small-scale* fading due to the movement of the UE, the movements of the

objects which have impacts on that particular path and even the microscopic changes in the air particles. Previously mentioned shadowing is a *large-scale* complement manifesting itself as birth or death of a path.

The *time-variance* of sparse channel parameters is a metric associated with the amount of signal spectral broadening caused by a Doppler shift which in return is proportional to the *effective* UE velocity in the direction of the coming path ray. The dual relation of a broadening in the frequency domain transfer function is a narrowing of the non-zero channel autocorrelation window in the time domain from infinity to a finite quantity known as channel *coherence time* T_o . The physical meaning of T_o is that when a sinusoid is transmitted twice at times t_1 and t_2 , the two are influenced differently by the channel if $\Delta t = |t_1 - t_2| \geq T_o$. The channel is very often considered as *fast-fading* when $T_o < T_c$ since in this case different parts of a chip are influenced by different-valued channel parameters. With this reasoning, CDMA channels always fall into the contrary *slow fading* category. A better criterion to judge whether a channel is fast or slow fading is to compare T_o with the delay requirements of the considered application or receiver block. If we consider a UE chip equalizer, for example, which recomputes its weights periodically from scratch by using the channel parameter estimates, then coherence time should be more than the chosen update period⁵.

One might think that slow fading is always a desired situation, however as explained before, it causes the deep fades to last very long. In some catastrophic cases none of the diversity measures might not help. Recently some work is going on to remedy such situations by artificially generating fast fading channel conditions via a transmission scheme called *opportunistic beamforming* [42].

Figure 10 gives a brief summary of the common channel impairments and the principal techniques for mitigating them.

⁵A typical requirement for the computation period of nonadaptive HSDPA equalizer weights is 512 chips

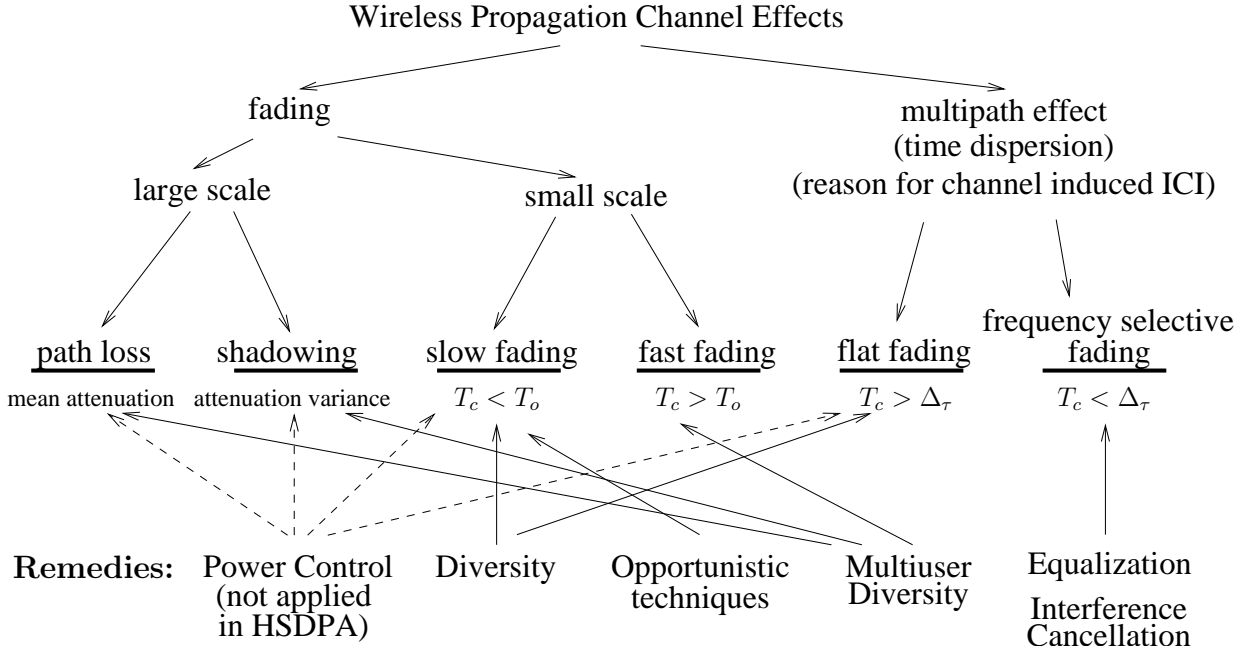


Figure 10: Summary of channel impacts and *most relevant* procedures against them.

0.3.2 HSDPA Signal Model

The discrete time counterpart of $h_{eff}(t)$ after the sampling operation becomes an FIR *multi-channel* $\mathbf{h}[l]$ or equivalently a *poly-phase* channel $\mathbf{h}_p[l]$ in the presence of multiple antennas and/or integer factor oversampling w.r.t. the chip rate as is shown in Figure 11. In such cases the received *vector stationary*⁶ signal can be modeled as the output of a $m \times 1$ single input multi output (SIMO) system⁷ with a past memory of $N - 1$ input elements and with the relations

$$\mathbf{y}[l] = \sum_{i=0}^{N-1} \mathbf{h}[i] b[l-i] + \mathbf{v}[l] \quad (6)$$

$$\mathbf{y}[l] = \begin{bmatrix} y_1[l] \\ \vdots \\ y_m[l] \end{bmatrix}, \mathbf{h}[l] = \begin{bmatrix} h_1[l] \\ \vdots \\ h_m[l] \end{bmatrix}, \mathbf{v}[l] = \begin{bmatrix} v_1[l] \\ \vdots \\ v_m[l] \end{bmatrix} \quad (7)$$

⁶meaning each phase is stationary

⁷although stationarity holds only for time-invariant channels we assume it also for the wireless channels considered in this text which vary slowly

where $\mathbf{v}[l]$ denotes the additive noise which represents the sum of the thermal noise and the intercell interference filtered by $p_r(t)$ and m denotes the product of the number of antennas and the oversampling factor. The multi-channel \mathbf{h} spanning N chips with $m \times 1$ chip rate elements, its poly-phase equivalent⁸ \mathbf{h}_p , the up-down flipped form $\bar{\mathbf{h}}_p$ and the poly-phase matched filter \mathbf{h}_p^\dagger in row vector format can be written as

$$\mathbf{h} = [\mathbf{h}[0], \mathbf{h}[1], \dots, \mathbf{h}[N-1]] \quad (8)$$

$$\mathbf{h}_p = \begin{bmatrix} \mathbf{h}[0] \\ \mathbf{h}[1] \\ \vdots \\ \mathbf{h}[N-1] \end{bmatrix}, \quad \bar{\mathbf{h}}_p = \begin{bmatrix} \mathbf{h}[N-1] \\ \mathbf{h}[N-2] \\ \vdots \\ \mathbf{h}[0] \end{bmatrix}, \quad \mathbf{h}_p^\dagger = \bar{\mathbf{h}}_p^H \quad (9)$$

Assuming $Q - 1$ interfering cells we can write as

$$\mathbf{y}[l] = \sum_{q=0}^{Q-1} \sum_{i=0}^{N-1} \mathbf{h}^{(q)}[i] b^{(q)}[l-i] + \mathbf{v}[l] \quad (10)$$

where index $q = 0$ denotes the own BS.

0.4 Suppression of Intracell Interference in HSDPA

Given the channel model discussed above for a single-cell system, we are now ready to discuss some typical receivers for general downlink CDMA systems and more specifically HSDPA that are designed to suppress intracell interference.

0.4.1 Rake Receiver and LMMSE Chip Equalizer

As shown in Figure 12, all the *linear* UE receivers can be mathematically represented in the form a common chip level filter followed by code specific correlators⁹.

⁸represented in a column format for compatibility with later formulations

⁹the order of the correlator and filtering can change like in the conventional Rake receiver

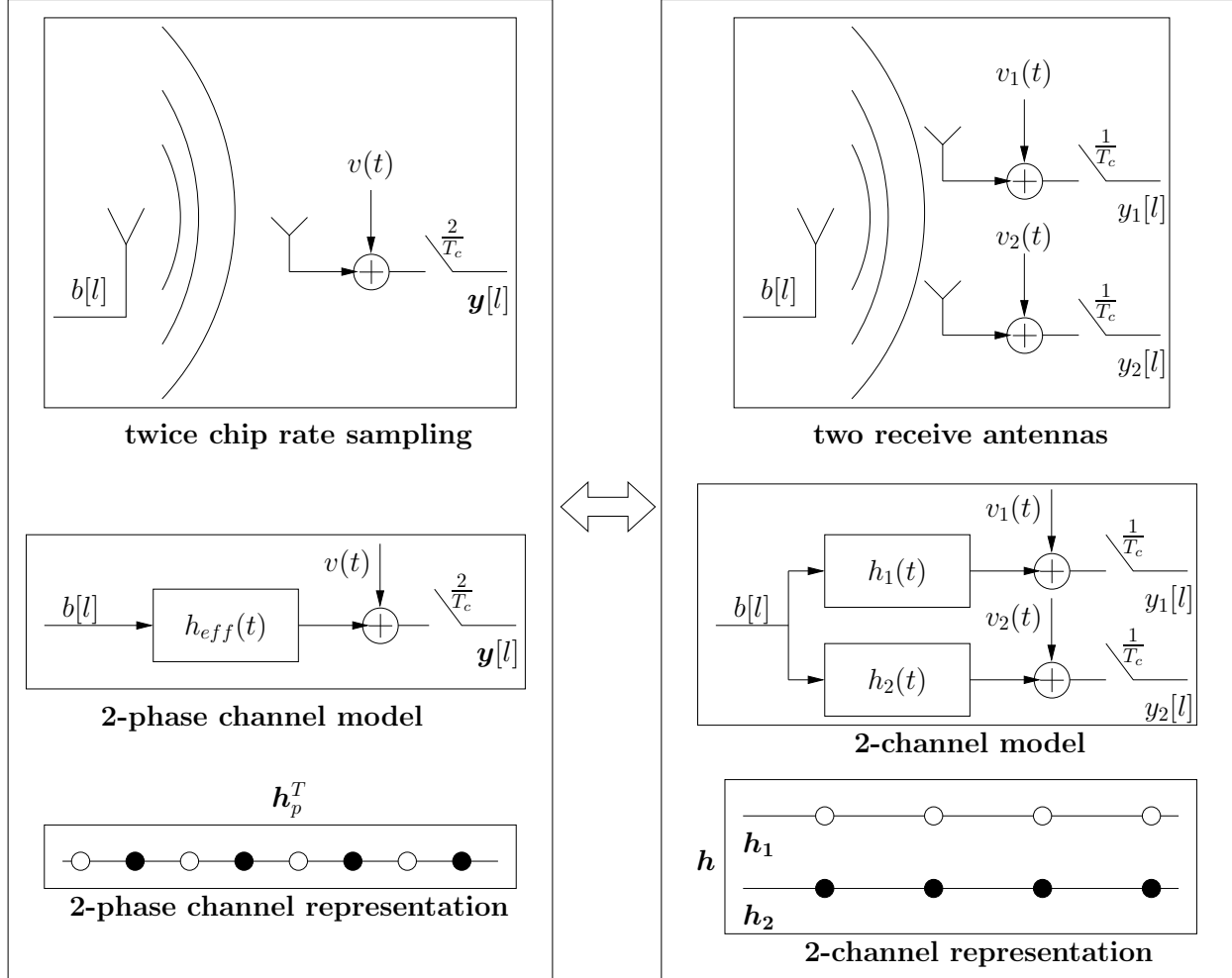


Figure 11: The equivalence of the poly-phase and the multi-channel models with a 2-phase example. It is possible to pass from one form to the other by P/S and S/P operations.

In order to motivate the discussion of this section, we consider the detection process of a *single* HSPDSCH user symbol $a_1[0]$ transmitted over the $L \times 1$ channelization code $\mathbf{c}_1 = \mathbf{c}_{16,0}$.

We consider a 2-phase linear filter which has a length of N chips which is the minimum length to deconvolve, i.e., to zero force, a 2-phase channel with a length of N chips.

We denote a block of the received signal as \mathbf{Y} and denote a block of the *total* transmitted chip sequence as \mathbf{B} whose elements are relevant to the estimation of the latter's subset $\mathbf{B}_0 = [b[L-1], \dots, b[0]]^T$ which overlaps with the period of the $a_1[0]$ symbol. \mathbf{Y} and \mathbf{B} are related by the $2(L+N-1) \times (L+2N-2)$ channel convolution matrix $\mathcal{T}(\mathbf{h})$ with the term

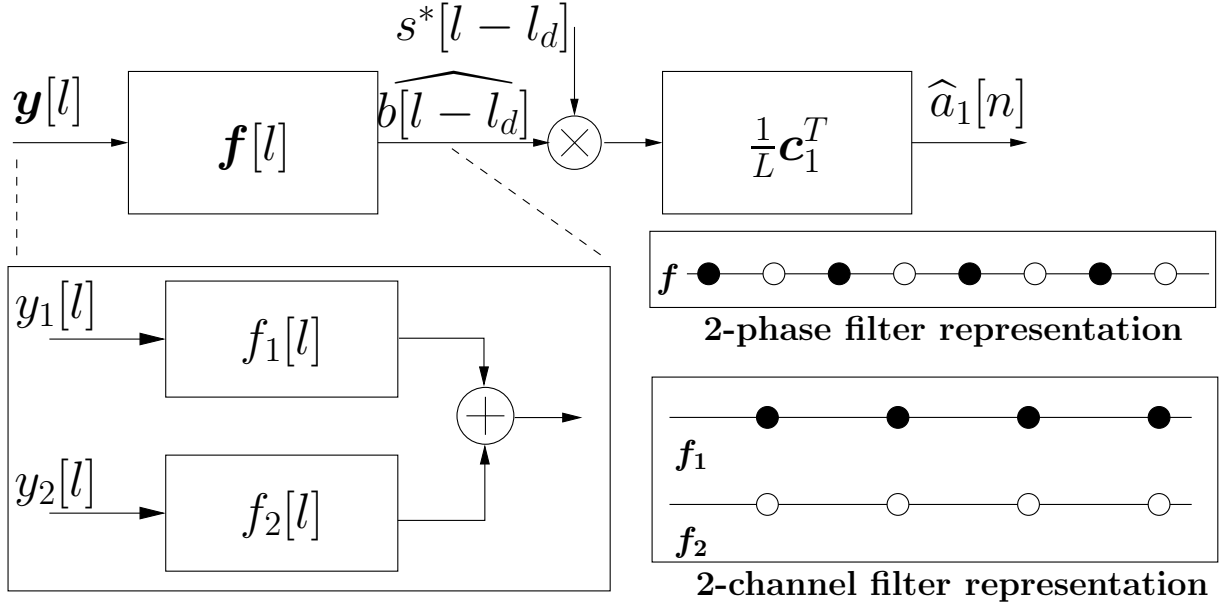


Figure 12: Receivers with linear *chip level filter - correlator* cascade. The order of the phases is reversed w.r.t. the channel phases order.

\mathbf{V} which is modeled as an additive white Gaussian noise (AWGN) representing the sum of the thermal noise and the intercell interference.

$$\mathbf{Y} = \mathcal{T}(\mathbf{h})\mathbf{B} + \mathbf{V} \quad (11)$$

$$= \begin{bmatrix} \mathbf{y}[L + N - 2] \\ \vdots \\ \mathbf{y}[0] \end{bmatrix} \quad (12)$$

$$\mathcal{T}(\mathbf{h}) = \begin{bmatrix} \mathbf{h}[0] & \dots & \mathbf{h}[N - 1] & \mathbf{0} & \mathbf{0} \\ \mathbf{0} & \ddots & \ddots & \ddots & \mathbf{0} \\ \mathbf{0} & \mathbf{0} & \mathbf{h}[0] & \dots & \mathbf{h}[N - 1] \end{bmatrix}, \quad \mathbf{V} = \begin{bmatrix} \mathbf{v}[L + N - 2] \\ \vdots \\ \mathbf{v}[0] \end{bmatrix} \quad (13)$$

$$\mathbf{B} = \sum_{k=1}^K \left[b_k[L + N - 2] \dots b_k[L - 1] \dots b_k[0] \dots b_k[-N + 1] \right]^T \quad (14)$$

K is the number of codes. The linear filter $f[l]$ is a 1×2 multi input single output (MISO)

system which turns the overall channel to a single input single output (SISO) system $\tilde{g}[l]$.

$$\mathbf{f} = [\mathbf{f}[0], \mathbf{f}[1], \dots, \mathbf{f}[N-1]], \quad \mathbf{f}[l] = [f[0], f[1]], \quad \tilde{g}[l] = \sum_{i=0}^l \mathbf{f}[i] \mathbf{h}_p[l-i] \quad (15)$$

The estimated BS chip sequence \mathbf{B}_0 can be formulated by the equations

$$\widehat{\mathbf{B}}_0 = \mathcal{T}(\mathbf{f})\mathbf{Y} = \mathcal{T}(\mathbf{f})\mathcal{T}(\mathbf{h})\mathbf{B} + \mathcal{T}(\mathbf{f})\mathbf{V} = \mathcal{T}(\mathbf{g})\mathbf{B} + \tilde{\mathbf{V}} \quad (16)$$

$$\mathcal{T}(\mathbf{f}) = \begin{bmatrix} \mathbf{f}[0] & \dots & \mathbf{f}[N-1] & \mathbf{0} & 0 \\ \mathbf{0} & \ddots & \ddots & \ddots & \mathbf{0} \\ 0 & \mathbf{0} & \mathbf{f}[0] & \dots & \mathbf{f}[N-1] \end{bmatrix}, \quad \tilde{\mathbf{V}} = \begin{bmatrix} \tilde{v}[L-1] \\ \vdots \\ \tilde{v}[0] \end{bmatrix} \quad (17)$$

$$\mathcal{T}(\mathbf{g}) = \begin{bmatrix} g[-N+1] & g[-N+2] & \dots & g[0] & \dots & g[N-1] & \mathbf{0} & 0 \\ \mathbf{0} & \ddots & \ddots & \ddots & \ddots & \ddots & \ddots & \mathbf{0} \\ 0 & \mathbf{0} & g[-N+1] & g[-N+2] & \dots & g[0] & \dots & g[N-1] \end{bmatrix} \quad (18)$$

where $\mathcal{T}(\mathbf{f})$ denotes the $L \times 2(L+N-1)$ filter convolution matrix, $\mathcal{T}(\mathbf{g})$ denotes the $L \times (L+2N-2)$ overall channel convolution matrix and $g[l] = \tilde{g}[l+N-1]$ reflects a variable change in order to better represent the precursor and postcursor parts of the overall channel the central tap of which corresponds to $g[0] = \mathbf{f}\bar{\mathbf{h}}_p$. The channel matched filter (CMF) $\mathbf{f} = \bar{\mathbf{h}}_p^H$ which is an equivalent of the filtering part of the conventional Rake receiver maximizes the SNR collecting all the channel energy to the central tap as $g[0] = \|\bar{\mathbf{h}}_p\|^2 = \|\mathbf{h}_p\|^2$. The unbiased form of CMF can be written as $\mathbf{f} = (\mathbf{h}_p^H \mathbf{h}_p)^{-1} \bar{\mathbf{h}}_p^H$.

Expanding (16), we reach to all the ingredients of $\widehat{\mathbf{B}}_0$ containing every user's chip sequences at different windows each scaled by the associated tap of the overall channel

$$\widehat{\mathbf{B}}_0 = \sum_{i=-N+1}^{N-1} g[i] \underbrace{\sum_{k=1}^K \mathbf{B}_{k,i}}_{\mathbf{B}_i} + \tilde{\mathbf{V}} \quad (19)$$

where $\mathbf{B}_{k,i} = [b_k[i+L-1], \dots, b_k[i]]^T$ and $b_k[i] = a_k \left\lfloor \frac{i}{L_k} \right\rfloor c_k[\text{mod}(i, L_k)] s[i]$.

The second stage correlation part of the receiver can be written as

$$\widehat{a_1[0]} = \frac{1}{L} \mathbf{c}_1^T \mathbf{S}_0^* \widehat{\mathbf{B}}_0 \quad (20)$$

where \mathbf{S}_i denotes a diagonal matrix with the scrambling elements $[s[L-1+i], \dots, s[i]]$ and the normalization by L is done to make up for the spreading-despreading gain.

Theorem 0.4.1 *The average SINR of the symbol estimate $\widehat{a_1[0]}$ by the usage of a general chip level linear filter \mathbf{f} is equal to*

$$\Gamma_1 = \frac{L |g(0)|^2 \sigma_{b_1}^2}{(\|\mathbf{g}\|^2 - |g(0)|^2) \sigma_b^2 + \|\mathbf{f}\|^2 \sigma_v^2} \quad (21)$$

where L is the spreading factor of the first user, \mathbf{g} is the impulse response of the channel filter cascade, $\sigma_{b_k}^2$ is the variance of the chips for user k and $\sigma_b^2 = \sum_{k=1}^K \sigma_{b_k}^2$.

Proof. First we give a useful relation

$$\frac{1}{L} \mathbb{E}\{\mathbf{c}_1^T \mathbf{S}_0^* \mathbf{S}_i \mathbf{c}_k^T\} = \begin{cases} 1 & i = 0, k = 1 \\ 0 & i = 0, k \neq 1 \\ \frac{1}{L} & i \neq 0 \end{cases} \quad (22)$$

The symbol estimate can be partitioned into four groups as

$$\widehat{a_1[0]} = \underbrace{g(0)a_1[0]}_{\text{signal}} + \underbrace{\frac{1}{L} \mathbf{c}_1^T \mathbf{S}_0^* g[0] \sum_{k=2}^K \mathbf{B}_{k,0}}_0 + \underbrace{\frac{1}{L} \mathbf{c}_1^T \mathbf{S}_0^* \left(\sum_{\substack{i=-N+1 \\ i \neq 0}}^{N-1} g[i] \sum_{k=1}^K \mathbf{B}_{k,i} \right)}_{\text{intracell interference}} + \underbrace{\frac{1}{L} \mathbf{c}_1^T \mathbf{S}_0^* \tilde{\mathbf{V}}}_{\text{noise}} \quad (23)$$

The first component which represents the useful signal part is the symbol of interest scaled by the central channel tap $g[0]$. The second component is zero since at the central tap instant $i = 0$, the scrambling and the descrambling blocks are aligned matching each-other, $\mathbf{S}_0^* \mathbf{S}_0 = \mathbf{I}_L$ and preserving the orthogonality among users

$$\mathbf{c}_1^T \mathbf{S}_0^* \mathbf{B}_{k,0} = \mathbf{c}_1^T \mathbf{S}_0^* \mathbf{S}_0 \mathbf{c}_k a_k[0] = \mathbf{c}_1^T \mathbf{c}_k a_k[0] = 0 \quad \forall k \neq 1 \quad (24)$$

The third *intracell* interference component represents the sum of ICI and MUI from the subcomponents with indices $k = 1$ and $k \neq 1$ respectively. The fourth component represents the noise contribution.

Taking the expected value of the symbol estimate power we obtain

$$\mathbb{E}|\hat{a}_1[0]|^2 = |g(0)|^2 \sigma_{a_1}^2 + \frac{1}{L} \sum_{\substack{i=-N+1 \\ i \neq 0}}^{N-1} |g[i]|^2 \sum_{k=1}^K \sigma_{a_k}^2 + \frac{1}{L} \|\mathbf{f}\|^2 \sigma_v^2 \quad (25)$$

where $\sigma_{a_k}^2$ represents the symbol variances, the noise power is amplified by the filter energy as is observed in the third component and the cross terms in the second component disappear by the expectation relation $\mathbb{E}\{a_k[0]a_l^*[0]\} = 0, k \neq l$.

Using the equalities $\|\mathbf{f}\|^2 \sigma_v^2 = \mathbf{f} \mathbf{R}_{vv} \mathbf{f}^H$ and $\|\mathbf{g}\|^2 = \mathbf{f} \mathcal{T}(\mathbf{h}) \mathcal{T}(\mathbf{h})^H \mathbf{f}^H$, $\sigma_{b_k}^2 = \sigma_{a_k}^2$ due to the fact the channelization codes are not normalized, we obtain

$$\begin{aligned} \mathbb{E}|\hat{a}_1[0]|^2 &= |g(0)|^2 \sigma_{a_1}^2 + \frac{1}{L} (\|\mathbf{g}\|^2 - |g(0)|^2) \sigma_b^2 + \frac{1}{L} \|\mathbf{f}\|^2 \sigma_v^2 \\ &= |g(0)|^2 \sigma_{a_1}^2 + \frac{1}{L} \mathbf{f} \left(\underbrace{\sigma_b^2 \mathcal{T}(\mathbf{h}) \mathcal{T}(\mathbf{h})^H + \mathbf{R}_{vv}}_{\mathbf{R}_{yy}} \right) \mathbf{f}^H - \frac{1}{L} |g(0)|^2 \sigma_b^2 \end{aligned}$$

Accordingly we reach to the SINR expression

$$\Gamma_1 = \frac{|g(0)|^2 \sigma_{a_1}^2}{\frac{1}{L} (\|\mathbf{g}\|^2 - |g(0)|^2) \sigma_b^2 + \frac{1}{L} \|\mathbf{f}\|^2 \sigma_v^2} \quad (26)$$

$$= \frac{|g(0)|^2 \sigma_{b_1}^2}{\frac{1}{L} (\|\mathbf{g}\|^2 - |g(0)|^2) \sigma_b^2 + \frac{1}{L} \|\mathbf{f}\|^2 \sigma_v^2} \quad (27)$$

$$= \frac{L |g(0)|^2 \sigma_{b_1}^2}{\mathbf{f} \mathbf{R}_{yy} \mathbf{f}^H - |g(0)|^2 \sigma_b^2} \quad (28)$$

□

Although the SINR expression is given as a metric for the estimation of symbols, in reality the linear filter \mathbf{f} estimates the BS chip sequence $b[l]$. Therefore the modified SINR expression

for the estimation of the BS chip sequence can be written as

$$\Gamma_c = \frac{|g(0)|^2 \sigma_b^2}{\mathbf{f} \mathbf{R}_{yy} \mathbf{f}^H - |g(0)|^2 \sigma_b^2} \quad (29)$$

where at the numerator, i.e., the useful energy part, there is no spreading gain and $\sigma_{b_1}^2$ is replaced by σ_b^2 .

The SINR metrics in (26) and (29) are based on the estimation of \mathbf{R}_{yy} statistics by taking expectation over the scrambler which is modeled as a random sequence and by using the orthogonality property of the codes. The receiver that maximizes these SINR metrics is the Max-SINR receiver which is more often known as chip level LMMSE receiver [20, 21].

Theorem 0.4.2 *The unbiased linear filter which achieves the maximum performance in terms of the SINR metric without exploiting the code and the power knowledge of the active users but by modeling the scrambling sequence as a random sequence and by taking expectations over it to approximate the received signal covariance matrix \mathbf{R}_{yy} is equal to [21]*

$$\mathbf{f}_o = \left(\bar{\mathbf{h}}_p^H \mathbf{R}_{yy}^{-1} \bar{\mathbf{h}}_p \right)^{-1} \bar{\mathbf{h}}_p^H \mathbf{R}_{yy}^{-1} \quad (30)$$

Proof. We first define the unbiasedness constraint as $g[0] = \mathbf{f}_o \bar{\mathbf{h}}_p = 1$. Then the optimization problem can be formulated as

$$\mathbf{f}_o = \arg_{\mathbf{f}_o \bar{\mathbf{h}}_p = 1} \max \Gamma_1 = \arg_{\mathbf{f}_o \bar{\mathbf{h}}_p = 1} \min \mathbf{f} \mathbf{R}_{yy} \mathbf{f}^H \quad (31)$$

The solution can be obtained by the standard Lagrange multiplier technique as follows:

$$\begin{aligned}
\Omega(\mathbf{f}^H, \mathbf{f}) &= \mathbf{f} \mathbf{R}_{yy} \mathbf{f}^H + 2\Re [\lambda (\mathbf{f} \bar{\mathbf{h}}_p - 1)] \\
\nabla_{\mathbf{f}} \Omega(\mathbf{f}^H, \mathbf{f}) &= \mathbf{f} \mathbf{R}_{yy} + \lambda \bar{\mathbf{h}}_p^H \\
&\Rightarrow \mathbf{f}_o = -\lambda \bar{\mathbf{h}}_p^H \mathbf{R}_{yy}^{-1} \\
\mathbf{f}_o \bar{\mathbf{h}}_p &= 1 \Rightarrow -\lambda \bar{\mathbf{h}}_p^H \mathbf{R}_{yy}^{-1} \bar{\mathbf{h}}_p = 1 \\
&\Rightarrow \lambda = \frac{-1}{\bar{\mathbf{h}}_p^H \mathbf{R}_{yy}^{-1} \bar{\mathbf{h}}_p} \\
&\Rightarrow \mathbf{f}_o = \frac{\bar{\mathbf{h}}_p^H \mathbf{R}_{yy}^{-1}}{\bar{\mathbf{h}}_p^H \mathbf{R}_{yy}^{-1} \bar{\mathbf{h}}_p} = \frac{\mathbf{h}_p^\dagger \mathbf{R}_{yy}^{-1}}{\mathbf{h}_p^\dagger \mathbf{R}_{yy}^{-1} \bar{\mathbf{h}}_p}
\end{aligned}$$

□

By taking an approximation of (30), we can obtain a slightly biased but simpler chip level LMMSE filter

$$\tilde{\mathbf{f}}_o = \sigma_b^2 \mathbf{h}_p^\dagger \mathbf{R}_{yy}^{-1} = \mathbf{R}_{by} \mathbf{R}_{yy}^{-1} \quad (32)$$

which fits to the Wiener filtering format.

Similar to the update from (6) to (10) if one has channel estimates of some other cells then a better performing chip equalizer expression can be obtained as

$$\tilde{\mathbf{f}}_o = \sigma_{b^{(0)}}^2 \mathbf{h}_p^{(0)\dagger} \left(\sum_{q=0}^{Q-1} \sigma_{b^{(q)}}^2 \mathcal{T}(\mathbf{h}^{(q)}) \mathcal{T}(\mathbf{h}^{(q)})^H + \mathbf{R}_{vv} \right)^{-1} \quad (33)$$

by modifying the \mathbf{R}_{yy} term¹⁰.

¹⁰This equalizer has the intercell interference suppression capability which will be elaborated more in later parts of the book chapter.

0.4.2 HSDPA Performance Analysis of Rake Receiver and Chip Equalizers

In this section we obtain the maximum achievable SINR and throughput performance metrics for various HSDPA service deployment scenarios while using the CMF and LMMSE equalizer type UE receiver components. The distributions of the radio channel parameters and the received powers from the own and surrounding base stations are modeled under correlated shadowing w.r.t. the mobile position, the cell radius and the type of environment. From such modeling, more realistic performance figures might be obtained as compared to fixing them to a selected set of values.

Hypothetical Receiver Models

We consider that possibly an interfering canceling (IC) structure is used in the first stage to cancel out intracell interference contributions of the PCPICH and HSPDSCHs.

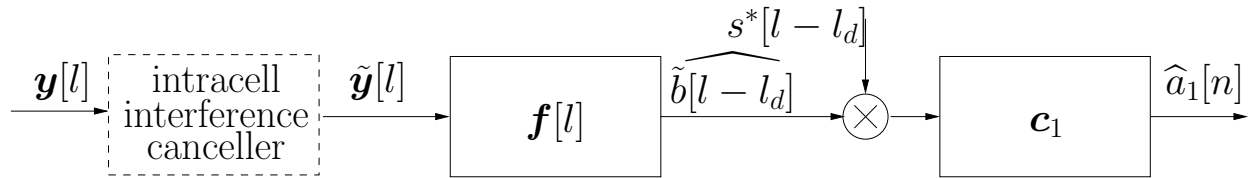


Figure 13: Hypothetical receiver model.

We assume that the residual BS signal $\tilde{b}[l]$ contained in the remaining sequence $\tilde{\mathbf{y}}[l]$ after the IC block is still block stationary and the second order intercell interference plus noise statistics σ_ν^2 is the same as before.

The modified SINR expression at the unbiased linear filter output, i.e., when $g[0] = 1$, for the symbol estimates of a single HSPDSCH channel of a UE situated at a particular position of the cell can be written as:

$$\Gamma_1 = \frac{16\rho P_0}{\left(\frac{1}{\alpha} - 1\right)\chi P_0 + \sum_{i=1}^6 P_i \|\mathbf{g}_i\|^2 + \|\mathbf{f}\|^2 \sigma_n^2} \quad (34)$$

where 16 is the HSPDSCH spreading gain. P_0 is the received power of the desired BS (BS 1),

there are K_1 HSPDSCH codes, ρ is the BS signal power portion of one HSPDSCH channel, χ is the remaining BS signal power portion after the IC block, P_i is the received powers from the i th cell among the 6 first-tier interfering unsectored cells¹¹ shown in Figure 1, \mathbf{g}_i is the convolution of the linear filter \mathbf{f} and the channel \mathbf{h}_i originating from the i th surrounding cell as $\mathbf{g}_i = \mathbf{f} * \mathbf{h}_i$ and σ_n^2 is the AWGN variance. AWGN term and intercell interference are treated separately for performance analysis purposes whereas they are treated similarly for filter adaptation due to the fact that it is impractical to incorporate in the signal model channel estimates and signal variances for a large number (6 here) of neighboring cells. As shown in the example of channel and CMF impulse responses in Figure 0.4.2, the term $\alpha = \frac{1}{\|\mathbf{g}\|^2}$ represents the ratio of the useful effective channel energy to the total effective channel energy and is known as the *orthogonality factor* which has been previously treated in the literature only for the RAKE receiver variants [29, 25].

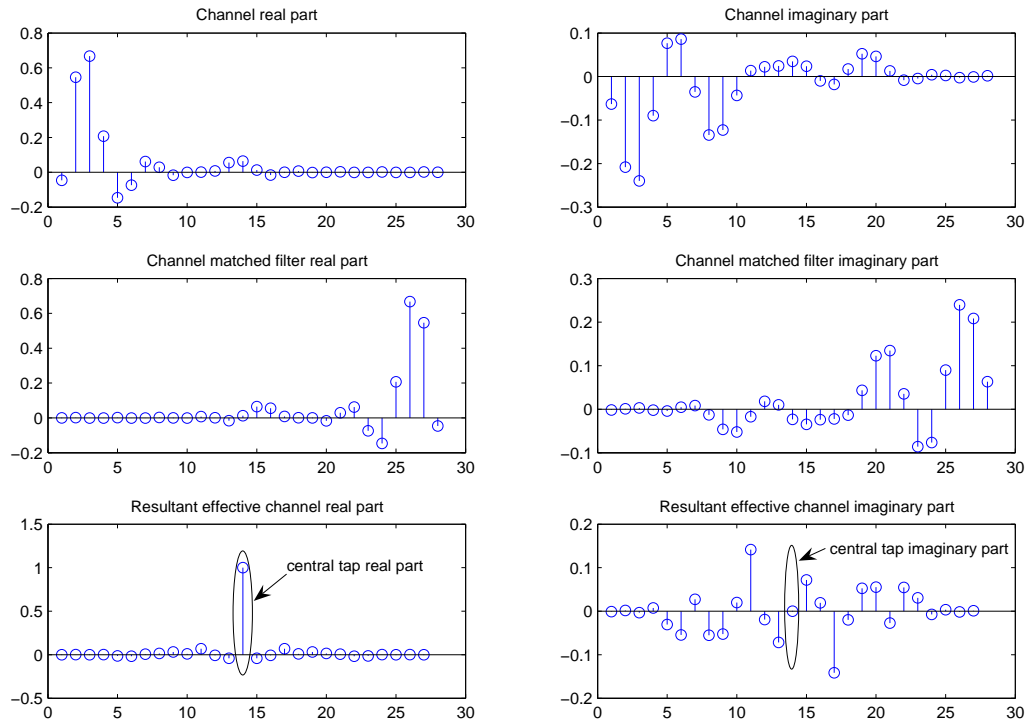


Figure 14: Orthogonality factor representation over an unbiased CMF. The central tap of the effective channel collects all the channel energy which is 1 due to unbiasedness. The cumulative energy of all the taps is $\|\mathbf{g}\|^2$.

¹¹the analysis done in this chapter is valid for also the sectored case

Parameter Modeling

We model all the parameters which appear in the SINR expression and which implicitly or explicitly depend on one or more of the location of the UE in the cell, the radius (r) of the cell and the type of the environment.

Modeling Received Powers

Received powers are calculated by the path loss and shadowing computations covered in section 0.3.1. As a single difference, for shadowing we first randomly generate a vector of seven independent shadowing values $\tilde{\mathbf{x}}$ of the own and first-tier six cells and turn it into a cross-correlated vector \mathbf{x} by left multiplying with the lower triangular Cholesky factorization output matrix \mathbf{L}_x of the symmetric shadowing correlation matrix \mathbf{R}_{xx} whose elements $\rho_{x_i x_j}$ given in Table 1 are obtained from the distance ratio dr_{ij} and the angle values θ_{ij} between the corresponding couples among the seven BSs and the UE as shown in Figure 15 [46].

$$\mathbf{R}_{xx} = \begin{bmatrix} \rho_{x_0, x_0} & \rho_{x_0, x_1} & \cdots & \rho_{x_0, x_6} \\ \rho_{x_1, x_0} & \rho_{x_1, x_1} & \cdots & \rho_{x_1, x_6} \\ \vdots & \vdots & \ddots & \vdots \\ \rho_{x_6, x_0} & \rho_{x_6, x_1} & \cdots & \rho_{x_6, x_6} \end{bmatrix} = \mathbf{L}_x \mathbf{L}_x^T, \quad \mathbf{x} = \mathbf{L}_x \tilde{\mathbf{x}} \quad (35)$$

Table 1: Shadowing correlation matrix elements

	$0 < \theta_{ij} < 30^\circ$	$30^\circ \leq \theta_{ij} < 60^\circ$	$60^\circ \leq \theta_{ij} < 90^\circ$	$90^\circ \leq \theta_{ij}$
$dr_{ij} \in [0, 2]$	$\rho_{x_i x_j} = 0.8$	$\rho_{x_i x_j} = 0.5$	$\rho_{x_i x_j} = 0.4$	$\rho_{x_i x_j} = 0.2$
$dr_{ij} \in [2, 4]$	$\rho_{x_i x_j} = 0.6$	$\rho_{x_i x_j} = 0.4$	$\rho_{x_i x_j} = 0.4$	$\rho_{x_i x_j} = 0.2$
$dr_{ij} \geq 4$	$\rho_{x_i x_j} = 0.4$	$\rho_{x_i x_j} = 0.2$	$\rho_{x_i x_j} = 0.2$	$\rho_{x_i x_j} = 0.2$

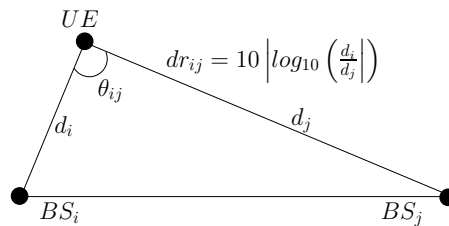


Figure 15: Distance and angle relations between two BSs and a UE.

Modeling Channel Parameters

The linear filter \mathbf{f} , the orthogonality factor α and the \mathbf{g}_i terms depend on the channel parameters for which we refer to Greenstein's channel model derived from the rms delay spread σ_{τ_i} and the power delay profile $P(\tau_i)$ [16]. Delay spread is equal to $\sigma_{\tau_i} = T_1 d^\epsilon y_i$ where T_1 is the reference delay spread at 1km distance from the BS, ϵ is the model parameter which is around 0.5 for almost all types of environments except very irregular mountainous terrains and y_i is a coefficient which is log-normally distributed with geometric mean 0 and geometric standard deviation σ_{y_i} . From field tests $\log(y_i)$ is also observed to be correlated with $\log(x_i)$ by a factor $\rho_{x_i y_i} = -0.75$, [16]. So we obtain the value of y_i from the correlation with the obtained shadowing value in the previous section. From the obtained delay spread we generate the power delay profile as $P(\tau_i) \propto e^{-\tau_i/\sigma_{\tau_i}}$ where \propto is the proportionality sign and τ_i values are the sampling instants. Since this is an infinite length sequence, we truncate it at the position where the final significant tap has 15 dB less power than the first tap. Then we pass the discrete power delay profile through *Rayleigh* fading to generate the *propagation* channel. The *transmission* channels are obtained by convolving the obtained propagation channels with the pulse shape and normalizing the result to unit energy.

Modeling χ

Among the common downlink channels, the pilot tone PCPICH has the highest interference with 10% BS power portion and it can be cancelled with high accuracy [35]. However it might be even more meaningful to consider cancelling the interference of HSPDSCH codes since by a highly probable deployment scenario, they will carry the majority (if not all) of the data traffic. We contemplate this because it would be easier to manage for an operator to dedicate one of its two or three carriers of 5 MHz. to the HSDPA service instead of distributing it over two or three available carriers. Furthermore there is no justified advantage of carrying high-rate data on a DCH with a very low spreading factor instead of on multiple HSPDSCHs. So, in the reception chain for a single HSPDSCH, we define five *perfect* first stage interference cancellation (IC) scenarios:

1. No interference canceller exists: $\chi = 1$

2. Pilot tone cancelled: $\chi = 0.9$
3. All the other HSPDSCHs cancelled: $\chi = 1 - (K_1 - 1)\rho$
4. Pilot+HSPDSCHs cancelled: $\chi = 0.9 - (K_1 - 1)\rho$
5. All intracell interference cancelled: $\chi = \rho$

Simulations Results

Five different environments are considered, the relevant parameters of which are shown in Table 2 which are adopted from COST231 propagation models [34] and from [16]. We fix transmitted BS power and AWGN power to $P_t = 43$ dBm and $\sigma_n^2 = -102$ dBm. Three different low-end to high-end HSDPA service scenarios are considered with $\{K_1, \rho\}$ sets as $\{1, 0.1\}, \{5, 0.06\}$ and $\{10, 0.06\}$. We uniformly position 10^4 UEs in one cell (home cell) and approximately that many more in an expanded region penetrating into other cells. This models the effect of shadowing resulting in handing off some UEs to other base stations despite their relatively greater distance as compared to the BS closest to the user. We also exclude a few closest points to the BS since otherwise the BS will serve only the closest UEs. For each node receiving the highest power from the BS of interest, we determine the relevant second-order statistics over 10 Rayleigh fading channel realizations. At each realization we obtain the SINR and spectral efficiency bound $\mathcal{C} = \log_2(1 + \Gamma_1)$ results for the CMF and LMMSE equalizer-correlator type receivers under the five above-mentioned interference cancellation scenarios. It was shown that the interference at the output of multiuser detectors can be approximated by a Gaussian distribution [47, 30]. Hence \mathcal{C} is an approximate Shannon capacity and it is a more meaningful measure than SINR since it defines the overall performance bound that can be achieved by the use of efficient transmission diversity, modulation and channel coding schemes. A number of spatio-temporal results on the order of 10^5 suffices to obtain the distribution of \mathcal{C} . Cumulative distributions of \mathcal{C} for 10 HSPDSCH codes deployment in the five reference environments are shown in Fig. 16 to Fig. 20. The calculated median values of \mathcal{C} for all the settings defined are tabulated in Table 3.

In the figures and the table, "C" represents CMF; "E" represents LMMSE equalizer-correlator receiver; suffixes to "C" and "E" ($\{1, \dots, 5\}$) represent in the same order the IC scenarios defined in section 0.4.2; {ind, umi, uma, sub} represent {indoor, urban microcell, urban macrocell, suburban macrocell} environments; the suffixes $\{1, 5, 10\}$ to these environments represent K_1 .

As observed in the figures, an increasing gap occurs between matched filtering results and equalization results when we go to user locations closer to the own BS which correspond to higher SINR regions. This is especially the valid case for indoor cells, urban microcells and urban macrocells where the eye is open for all user locations since white noise (thermal noise and partially intercell interference) suppressing CMF is much more effected by the intracell interference most of which however is suppressed when an equalizer is used and the need for an IC decreases. In other words, in such environments orthogonality factors at the output of LMMSE equalizers are much higher than those of CMFs.

In the suburban macrocell sizes, for the most distant 30% cellular positions, there is no difference in the performance of receivers. When we further go to the extreme rural cell sizes, there is almost no difference except at a small number of very close UE positions. These figures clearly show the dominance of multiuser interference in small cells where using interference suppressing equalizers becomes meaningful and the dominance of AWGN in the large cells where CMF or RAKE receiver is sufficient.

According to UMTS deployment scenarios, more than 80% of UMTS cells will be pico or micro cells and hence it will certainly pay off if a UE considers the LMMSE equalizer in order to be scheduled for a high SINR demanding HSDPA service. In these settings, the achievable *maximum C* by using equalizers is approximately twice that of CMFs. So, in an ideal condition, CMF has less chance of providing a very high rate demanding application.

In Table 3, we notice that when an equalizer is used, the median capacity for a UE increases when we move from indoor to urban environments which is mostly because of the trend of path-loss exponent. When it is low, intercell interference will be high. However as we further increase the size of the cell, AWGN starts to dominate and median capacity decreases. We also see that w.r.t. CMF, equalizers alone improve the median capacity of

pico and micro cells between 60% and 115%. When complete interference cancellation is achieved these figures increase to 98% and 199%.

Cancelling the pilot tone alone brings very little gain. Moshavi et.al however claim that it is possible to obtain 11% capacity gain by cancelling the 10% power pilot tone since this much cancelled power can be exploited by the BS to accept a proportional number of new users [36]. This can be only valid if all the UE receivers at the same time cancel the pilot tone which is not dictated for the moment by the standard. Nevertheless when equalization is used, it is more worthwhile to subtract known non-orthogonal channels, e.g., the synchronization channels. We shall however not discuss this aspect any further due to space limitations.

Note that the results obtained are valid when there is no LOS and surrounding cells have identical properties. In reality, we expect higher capacity from picocellular regions since they will be some isolated hot zones like airports and there will be a higher probability of LOS. Furthermore, note that capacity we are concerned with here is the single cell capacity. Of course, global system capacity from the adoption of picocells will be much higher than others since there will be more cells and hence more users will be served.

Table 2: Cellular deployment scenarios

PARAMETERS	G_1	n	r	T_1	σ_x	σ_y
Indoor	138	2.6	0.2	0.4	12	2
Urbanmicro	131	3	0.5	0.4	10	3
Urbanmacro	139.5	3.5	1	0.7	8	4
Suburbanmacro	136.5	3.5	2	0.3	8	5
Rural	136.5	3.85	8	0.1	6	6

Table 3: Throughput bound median results

\mathcal{C}	C1	C2	C3	C4	C5	E1	E2	E3	E4	E5
ind1	2.46	2.54	2.46	2.54	4.54	3.94	3.99	3.94	3.99	4.87
ind5	1.86	1.94	2.09	2.21	4.13	3.22	3.27	3.33	3.42	4.34
ind10	1.86	1.96	2.53	2.73	4.11	3.31	3.35	3.63	3.73	4.30
umi1	2.18	2.29	2.18	2.29	4.54	4.16	4.20	4.16	4.20	5.30
umi5	1.65	1.74	1.89	2.02	4.34	3.56	3.59	3.71	3.77	4.94
umi10	1.70	1.79	2.41	2.63	4.32	3.59	3.63	4.00	4.16	4.95
uma1	1.78	1.88	1.78	1.88	4.13	3.80	3.86	3.80	3.86	5.16
uma5	1.30	1.37	1.50	1.62	3.97	3.09	3.14	3.26	3.35	4.72
uma10	1.30	1.38	1.95	2.15	3.91	3.10	3.17	3.58	3.74	4.50
sub1	1.11	1.17	1.11	1.17	1.60	1.40	1.42	1.40	1.42	1.61
sub5	0.79	0.82	0.87	0.91	1.19	1.02	1.03	1.05	1.06	1.19
sub10	0.77	0.81	0.97	1.02	1.18	0.98	1.00	1.07	1.09	1.18

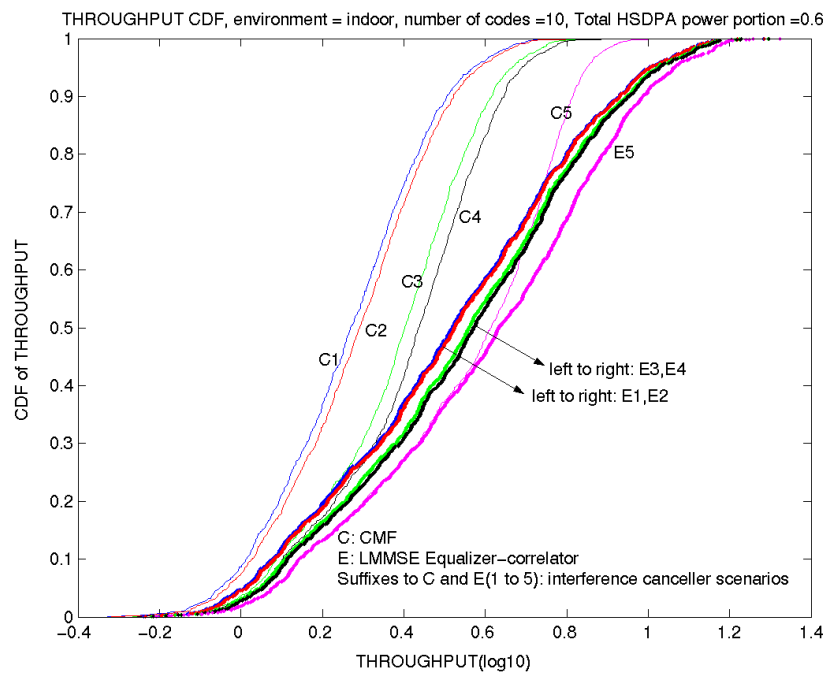


Figure 16: Throughput bound CDF of indoor microcell.

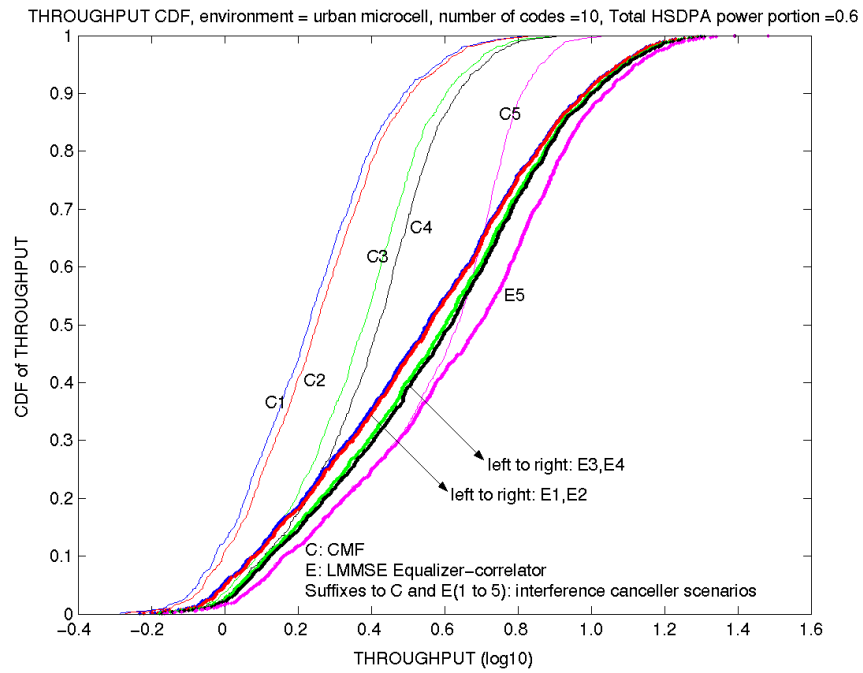


Figure 17: Throughput bound CDF of urban microcell.

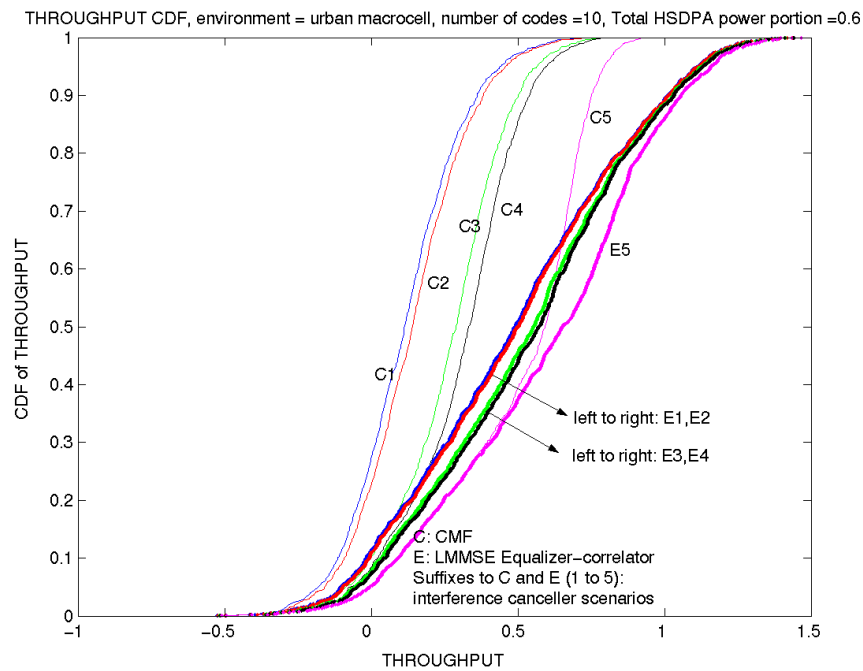


Figure 18: Throughput bound CDF of urban macrocell.

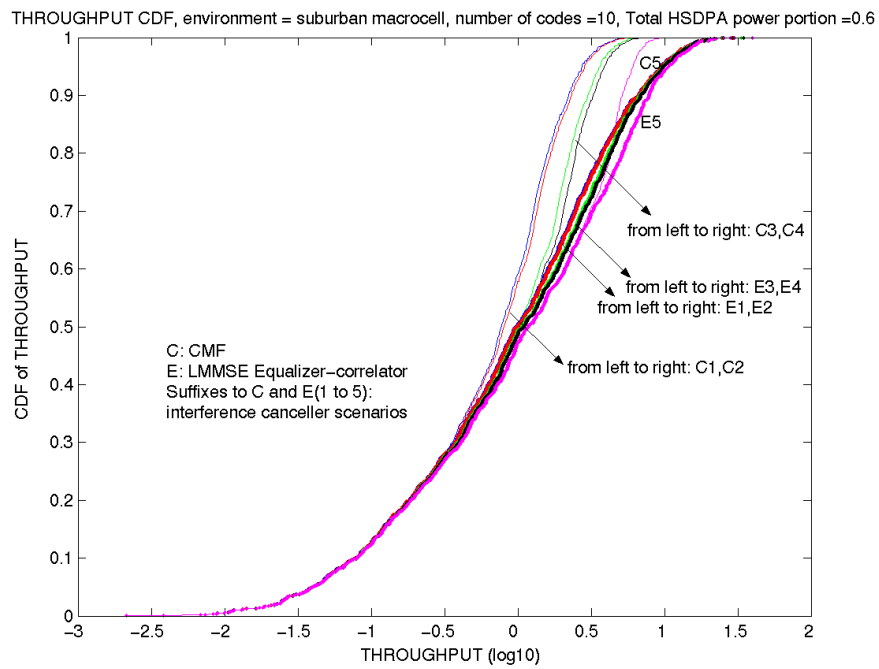


Figure 19: Throughput bound CDF of suburban macrocell.

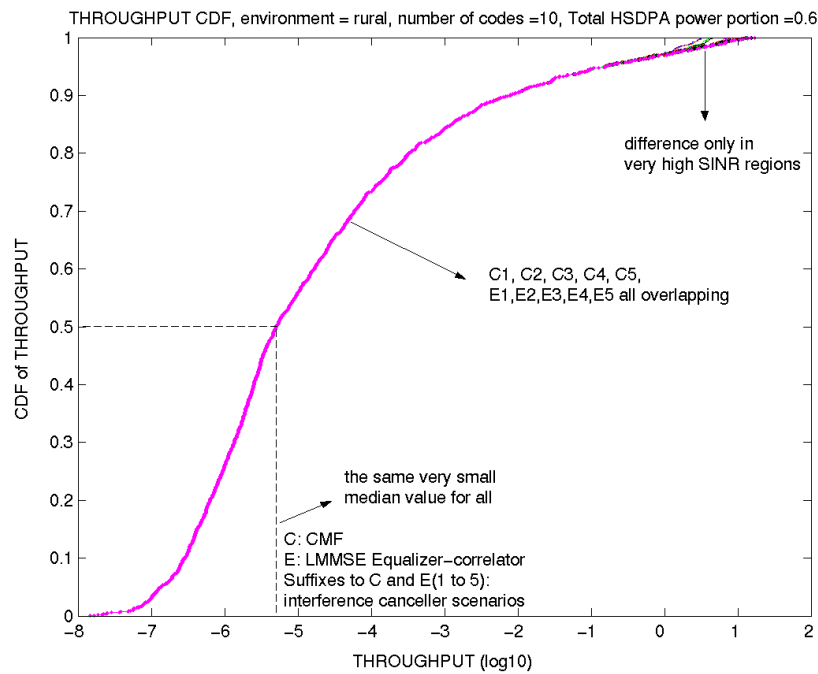


Figure 20: Throughput bound CDF of rural cell.

0.5 Advanced Receivers for Interference Cancellation

Chip-level equalization happens to be a solution of interest for the very specific case of downlink synchronous CDMA. When multiuser interference is of a more general nature e.g., due to asynchronous or non-orthogonal downlink codes, the solutions for its suppression are equivalently more general and are labelled as *multiuser* receivers or detectors. We discuss some well-documented multiuser receivers in this section and later apply them to the specific case of suppression of intercell interference in HSDPA downlink.

0.5.1 Symbol-Rate Signal Model

The signal model in (10) is a chip-rate model where $b^{(q)}[i]$ is the i th chip from the q th base station. We can write the equivalent discrete-time signal model at the symbol-rate as

$$\mathbf{Y}[n] = \sum_{q=0}^{Q-1} \overbrace{\mathcal{T}(\mathbf{h}^{(q)})\mathbf{S}^{(q)}[n]\mathbf{C}}^{\tilde{\mathbf{G}}^{(q)}[n]} \mathbf{A}^{(q)}[n] + \mathbf{V}[n] \quad (36)$$

where K is the number of users assumed without loss of generality the same from all base stations, $\mathbf{Y}[n]$ represents the received data block spanning the channel output corresponding to transmission of M symbols at time instant n , $\tilde{\mathbf{G}}^{(q)}[n]$ is the symbol rate channel¹² from base station q composed of the cascade of the propagation channel $\mathcal{T}(\mathbf{h}^{(q)})$, the diagonal scrambling code matrix $\mathbf{S}^{(q)}[n]$ and the block-diagonal channelization code matrix \mathbf{C} , assumed to be the same for all base stations. $\mathbf{A}^{(q)}[n]$, represents the unit-amplitude MK desired symbols vector. Since the nature of intracell and intercell interference is the same (non-orthogonal), we shall assume in the interest of clarity, only one base station $Q = 1$ and suppress the index q for the purposes of the following discussion.

¹²time-varying since it includes the scrambler

0.5.2 Optimal Receiver

The optimal multiuser detector in terms of minimum symbol error rate (SER) is the Maximum Likelihood Sequence Estimation (MLSE) which is an exhaustive search procedure over the symbol alphabets of all the possible transmitted sequences of all the users with the minimization criterion [22]

$$\hat{\mathbf{A}}_{ML} = \arg \min_{\mathbf{A} \in \mathcal{X}^{MK}} \left\| \mathbf{Y} - \overbrace{\mathbf{T}(\mathbf{h})\mathbf{S}\mathbf{C}}^{\tilde{\mathbf{G}}}\mathbf{A} \right\|^2 \quad (37)$$

where, \mathcal{X} denotes the symbol alphabet¹³. Since this criterion is finite-alphabet constrained, it is NP-hard¹⁴ and perhaps the best that can be done is to use the Viterbi algorithm which is also exponentially complex with the factor MK [44]. Due to these reasons, ML receiver is mostly considered as not implementable and its performance serves only as an upper-bound. Furthermore, in case of signals from multiple base station, ML detection of all symbols from all base stations must be considered making the solution even more undesirable in the downlink problem. Note that (37) is at the same time the nonlinear LS estimator¹⁵.

0.5.3 Decorrelating Receiver

One of the suboptimal but simpler approaches is to relax the finite alphabet constraint mapping of \mathbf{A} from the finite set \mathcal{X}^{MK} into \mathbb{C}^{MK} which turns the nonlinear LS problem in (37) into a linear LS problem

$$\hat{\mathbf{A}}_{LS} = \arg \min_{\mathbf{A} \in \mathbb{C}^{MK}} \left\| \mathbf{Y} - \tilde{\mathbf{G}}\mathbf{A} \right\|^2 \quad (38)$$

whose solution is

$$\hat{\mathbf{A}}_{LS} = \tilde{\mathbf{F}}_{Dec}\mathbf{Y} = \left(\overbrace{\tilde{\mathbf{G}}^H\tilde{\mathbf{G}}}^{\mathbf{R}} \right)^{-1} \tilde{\mathbf{G}}^H\mathbf{Y} = \mathbf{R}^{-1}\mathbf{X} \quad (39)$$

¹³representing the simple case of same constellation for all users

¹⁴a decision problem which is at least as hard as any problem whose solution can be *verified* by polynomial complexity

¹⁵in statistical terms, LS is *disguised* ML when the measurement noise sequence \mathbf{V} is zero-mean, *i.i.d.* and Gaussian

where \mathbf{X} and \mathbf{R} respectively denote the single user matched filter (SUMF) bank output symbol estimates and their cross-correlation matrix.

An equivalent model in terms of linear systems of equations can be written as

$$\mathbf{R}\hat{\mathbf{A}}_{LS} = \mathbf{X} \quad (40)$$

Note that LS estimator treats the elements of \mathbf{A} vector as deterministic unknown parameters having diffuse prior pdfs.

LS estimation, i.e. decorrelation, is the unique least MSE member of the ZF MUDs (thus called MMSE-ZF receiver) set with the general members expressed as

$$\hat{\mathbf{A}}_{ZF} = (\mathbf{T}\tilde{\mathbf{G}})^{-1} \mathbf{T}\mathbf{Y}$$

with any proper \mathbf{T} matrix.

Projection Interpretation of Decorrelating Receiver

Projection receiver is another name for the symbol-level MMSE-ZF. It was first presented as the projection receiver for CDMA communications by Schlegel et al. in [37] and is based on suppressing both inter-cell and intra-cell interference by projecting the undesired users onto the subspace orthogonal to the one spanned by the desired user's signal vector. We will propose different approaches for both exact and approximated interference projection.

Considering the symbol-level model,

$$\mathbf{Y}[n] = \tilde{\mathbf{G}}[n]\mathbf{A}[n] + \mathbf{V}[n] \quad (41)$$

We call $a[n]$ the symbol to estimate, $\tilde{\mathbf{g}}[n]$ the column of $\tilde{\mathbf{G}}[n]$ corresponding to that symbol and $\tilde{\mathbf{G}}[n]$ all the other columns of $\tilde{\mathbf{G}}[n]$. Inter-symbol interference, inter-cell interference and

intra-cell interference are all included into $\bar{\mathbf{G}}[n]$. We can write the received signal as:

$$\mathbf{Y} = \tilde{\mathbf{g}}[n]a[n] + \bar{\mathbf{G}}[n]\bar{\mathbf{A}}[n] + \mathbf{V}[n] \quad (42)$$

From a geometrical point of view the columns of $\bar{\mathbf{G}}[n]$ span a certain subspace, the *interference subspace*. $\mathcal{S} = \text{span}(\bar{\mathbf{G}}[n])$ where $\text{span}(\cdot)$ generates all possible linear combinations of the vectors inside the brackets. We define the projection matrix:

$$\mathbf{P}_{\bar{\mathbf{G}}[n]} = \bar{\mathbf{G}}[n] (\bar{\mathbf{G}}^H[n]\bar{\mathbf{G}}[n])^{-1} \bar{\mathbf{G}}^H[n] \quad (43)$$

being the unique orthogonal projection onto \mathcal{S} , i.e., for any $\mathbf{x} \in \mathbb{C}^{\mathcal{D}}$ then $\mathbf{P}_{\bar{\mathbf{G}}[n]}\mathbf{x} \in \mathcal{S}$ and $\|\mathbf{x} - \mathbf{P}_{\bar{\mathbf{G}}[n]}\mathbf{x}\|^2$ is minimal. \mathcal{D} is the dimension of the vector \mathbf{x} . Further, we define:

$$\mathbf{P}_{\bar{\mathbf{G}}[n]}^\perp = \mathbf{I} - \mathbf{P}_{\bar{\mathbf{G}}[n]} = \mathbf{I} - \bar{\mathbf{G}}[n] (\bar{\mathbf{G}}^H[n]\bar{\mathbf{G}}[n])^{-1} \bar{\mathbf{G}}[n]^H \quad (44)$$

which is the projection matrix on \mathcal{S}^\perp (the orthogonal complement of \mathcal{S}), so that for any $\mathbf{x} \in \mathbb{C}^{\mathcal{D}}$ then $\mathbf{P}_{\bar{\mathbf{G}}[n]}^\perp\mathbf{x} \in \mathcal{S}^\perp$.

As the vector obtained in this way has no components in the interference subspace, a simple matched filter ($\tilde{\mathbf{g}}^H[n]$) suffices to retrieve the transmitted symbol $a[n]$. Up to a proper scalar scaling factor, the result obtained may be shown to be equivalent to the result obtained by a symbol-level MMSE-ZF equalizer.

$$\hat{a}[n] = \frac{1}{\tilde{\mathbf{g}}^H[n]\mathbf{P}_{\bar{\mathbf{G}}[n]}^\perp\tilde{\mathbf{g}}[n]}\tilde{\mathbf{g}}^H[n]\mathbf{P}_{\bar{\mathbf{G}}[n]}^\perp\mathbf{Y} \quad (45)$$

While the classical expression for the MMSE-ZF filter would be:

$$\hat{a}^{ZF}[n] = \mathbf{e}_n^T (\tilde{\mathbf{G}}^H[n]\tilde{\mathbf{G}}[n])^{-1} \tilde{\mathbf{G}}^H[n]\mathbf{Y} \quad (46)$$

where \mathbf{e}_n is a unit vector.

Notice that both symbol-level MMSE ZF receiver and projection receiver need the matrix $\tilde{\mathbf{G}}[n]$ (or $\bar{\mathbf{G}}$) to be *tall* to have enough degrees of freedom for the inversion. In general if

the number of interferers is not too large (intracell codes as well as intercell interference) the model (41) allows leveraging on the stacking factor (increasing M) to arbitrarily increase the number of rows of the matrix.

Successive Projection Algorithms

Most of the computational complexity of the projection receiver lies in the inversion of the Gramian term $\bar{\mathbf{G}}^H[n]\bar{\mathbf{G}}[n]$, which is a square matrix whose dimension is equal to the total number of interfering columns, J .

In order to avoid performing the inverse, one simplification can be represented by the idea of projecting the received signal successively on each one of the columns that compose $\bar{\mathbf{G}}[n]$, $\bar{\mathbf{g}}_1[n]$ till $\bar{\mathbf{g}}_J[n]$. Doing it vector by vector, the Gramian terms result in a scalar (the squared norm of the considered vector) and the inversion becomes simply a division by a scalar. The resulting iterative algorithm is the following:

$$\begin{aligned} \mathbf{Y}^{(0)} &= \mathbf{Y}[n] \\ \text{for } i &= 1 : J \rightarrow \mathbf{Y}^{(i)} = \mathbf{Y}^{(i-1)} - \frac{1}{\|\bar{\mathbf{g}}_i[n]\|^2} \bar{\mathbf{g}}_i[n] \bar{\mathbf{g}}_i^H[n] \mathbf{Y}^{(i-1)} \\ \hat{a}_n &= \tilde{\mathbf{g}}^H[n] \mathbf{Y}^{(J)} \end{aligned} \tag{47}$$

This algorithm allows a considerable reduction in complexity compared to the full matrix projection. However projecting vector by vector separately like this is an *approximation* of the full matrix projection exposed above. The two methods would be equivalent *if and only if* the columns $\tilde{\mathbf{g}}_i[n]$ were *orthogonal*. This condition can be achieved by applying a prior orthonormalization process onto the considered vectors, via Gram-Schmidt procedure or an equivalent one. The one implemented here is a modified version of the Gram-Schmidt procedure, in which the computation of square roots is avoided (square roots have a consistent computational complexity). In fact for our purposes the normalization of the basis is not needed. In this way a matrix \mathbf{U} is computed, whose columns form an orthogonal basis for the interference subspace \mathcal{S} and it is on these vectors that the projections are done. The

orthogonalization process is provided as follows.

$$\begin{aligned}
 \mathbf{u}_1 &= \bar{\mathbf{g}}_1[n] \\
 \text{for } i = 2 : J &\rightarrow \mathbf{u}_i = \bar{\mathbf{g}}_i[n] - \sum_{k=1}^{i-1} c_{k,i} \mathbf{u}_k \\
 \text{where } c_{k,i} &= \langle \mathbf{u}_k, \bar{\mathbf{g}}_i[n] \rangle
 \end{aligned} \tag{48}$$

If one basis vector \mathbf{u}_i is too small (norm lower than a certain value ε) it is discarded. This means that the rank of the interference matrix $\bar{\mathbf{G}}[n]$ is lower than J . Once all the vector of the basis have been computed, the projection is done on these vectors exactly as in the previous case (47).

The orthogonalization process allows to have an *exact* projection algorithm even if performed vector by vector. However it introduces an additional complexity compared to the direct projection on the columns $\bar{\mathbf{G}}[n]$. So both approaches are reasonable, depending on which trade-off between performances and complexity one wants to achieve. The loss in performances deriving from the first approach depends mainly on two factors:

1. how *sparse* is the matrix $\bar{\mathbf{G}}[n]$
2. how *tall* is the matrix $\bar{\mathbf{G}}[n]$

In fact, the more the matrix tends to have such characteristics, the more the inner product between pairs of its columns tends to be small and therefore the condition of orthogonality is approached. Often in practical cases this situation is verified (small number of codes and small number of interfering base stations to cancel) and thus there is no particular need for a prior orthogonalization process since the gap in performance is not enormous.

Projections on Reduced Subspaces

To reduce even more the complexity, one can exploit the fact that not all the interfering

vectors $bm\bar{g}_i[n]$ contribute in an equal way to the interference. So the number of vectors to consider can be reduced from the full number J down to a certain subset of *strongest* interferers.

One criterion for the selection of these vectors can be represented by their *inner product* with the column $\tilde{\mathbf{g}}[n]$: in this case, we fix a certain threshold ϑ ; if the inner product between the columns $\bar{\mathbf{g}}_i[n]$ and $\tilde{\mathbf{g}}[n]$ is greater than ϑ , the columns will be included in the projection subset, otherwise it will be discarded. The proposed algorithm behaves as follows:

$$\begin{aligned}
& \mathbf{Y}^{(0)} = \mathbf{Y}[n] \\
& \text{for } i = 1 : J \\
& \quad \text{if } \langle \bar{\mathbf{g}}_i[n], \tilde{\mathbf{g}}[n] \rangle \geq \vartheta \rightarrow \mathbf{Y}^{(i)} = \mathbf{Y}^{(i-1)} - \frac{1}{\|\bar{\mathbf{g}}_i[n]\|^2} \bar{\mathbf{g}}_i[n] \bar{\mathbf{g}}_i^H[n] \mathbf{Y}^{(i-1)} \\
& \text{end} \\
& \hat{a}_n = \tilde{\mathbf{g}}[n]^H \mathbf{Y}^{(J)}
\end{aligned} \tag{49}$$

Simulations results show that a proper choice for ϑ can be around 0.2. Furthermore, if the number of selected columns is not very high on the average, it is also possible to make the projection on the whole matrix formed by these vectors, which will give better performances.

0.5.4 LMMSE Receiver

Although complete deconvolution is possible for $\tilde{\mathbf{G}}$ with the decorrelator $\tilde{\mathbf{F}}_{Dec}$, it amplifies the noise term \mathbf{V} . A better approach is the LMMSE estimator which models \mathbf{A} as a random Gaussian vector and solves the cost criterion

$$\tilde{\mathbf{F}}_{LMMSE} = \arg_{\tilde{\mathbf{F}}} \min_{\mathbf{A} \in \mathbb{C}^{MK}} \mathbb{E} \left(\tilde{\mathbf{F}} \mathbf{Y} - \mathbf{A} \right) \left(\tilde{\mathbf{F}} \mathbf{Y} - \mathbf{A} \right)^H \tag{50}$$

with the solution

$$\tilde{\mathbf{F}}_{LMMSE} = \left(\tilde{\mathbf{G}}^H \tilde{\mathbf{G}} + \mathbf{R}_{VV} \right)^{-1} \tilde{\mathbf{G}}^H \quad (51)$$

which different from the decorrelator requires also the noise covariance matrix symbol amplitudes \mathbf{R}_{VV} . Note that for vanishing noise $\tilde{\mathbf{F}}_{LMMSE}$ becomes equivalent to the decorrelator. For high noise, on the other hand, it is identical to the single-user matched filter (SUMF).

The equivalent model in terms of linear systems of equations can be written as

$$\underbrace{(\mathbf{R} + \mathbf{R}_{VV})}_{\mathbf{T}} \hat{\mathbf{A}}_{LMMSE} = \mathbf{X} \quad (52)$$

where \mathbf{T} denotes the SUMF bank output covariance matrix. Both decorrelator and LMMSE receiver are very complex due to the fact they require matrix-inversion operations with $O(M^3K^3)$ complexity. Therefore reduced rank approximations of the matrix inversion operation have been investigated in literature with iterative techniques. We will elaborate on only the so-called Parallel Interference Cancellation (PIC) family which is the counterpart of Jacobi iterations for the iterative solutions of linear systems of equations since it works particularly well when user symbols have similar power levels which is the case for HSDPA. For other state of the art iterative techniques which are not discussed here such as Successive Interference Cancellation (SIC) which is the counterpart of Gauss-Seidel iterations in matrix algebra or the Decorrelating Decision Feedback Equalizer (DFE) see [43] and [11].

0.5.5 Linear Parallel Interference Cancellation Receiver

Conventional LPIC corresponds to using Jacobi iterations for the solutions of linear system of equations [40]. Splitting the \mathbf{R} expression in (40) into the two parts as \mathbf{I} and $(\mathbf{R} - \mathbf{I})$ one can reach to the iterative decorrelation solution as¹⁶

$$\hat{\mathbf{A}}_{LS}^{(i)} = (\mathbf{I} - \mathbf{R}) \hat{\mathbf{A}}_{LS}^{(i-1)} + \mathbf{X} \quad (53)$$

¹⁶similarly splitting \mathbf{T} in (52) for the LMMSE receiver

The iterations converge provided that the spectral radius $\rho(\mathbf{I} - \mathbf{R})$ is less than 2, which is not guaranteed¹⁷.

A better approach is to tackle the problem from Cayley-Hamilton theorem which states that every square matrix satisfies its characteristic equation. This principle can be used to find the inverse of an $n \times n$ square matrix by a polynomial expansion as [9]

$$\begin{aligned}
 \det(\mathbf{R} - \lambda\mathbf{I}) &= 0 \\
 \Rightarrow 1 - c_1\lambda - \dots - c_{n-1}\lambda^{n-1} - c_n\lambda^n &= 0 \\
 \Rightarrow \mathbf{I} - c_1\mathbf{R} - \dots - c_{n-1}\mathbf{R}^{n-1} - c_n\mathbf{R}^n &= \mathbf{0} \\
 \Rightarrow \mathbf{I} = c_1\mathbf{R} + \dots + c_{n-1}\mathbf{R}^{n-1} + c_n\mathbf{R}^n & \\
 \Rightarrow \mathbf{R}^{-1} = c_1\mathbf{I} - \dots + c_{n-1}\mathbf{R}^{n-2} + c_n\mathbf{R}^{n-1} &
 \end{aligned}$$

With polynomial expansion it is possible to obtain the decorrelator solution or the LMMSE solution in n iterations. Suboptimal solutions are obtained by stopping at a few iterations in which case the optimal weights change as well. Although this looks like an attractive solution at first sight, the complexity depends on the weight adaptation. See [26] and [27] for two adaptation schemes one from the direct derivation from the MMSE expression for a particular number of iterations and one from large system analysis respectively. In this text we are not concerned with weight adaptation but instead with filter adaptation.

0.5.6 Iterative Receivers based on Chip Equalizers

The LMMSE chip equalizer-correlator receiver does not exploit subspaces in partially loaded systems. This is in contrast to the symbol level LMMSE receiver, which as discussed below is time-varying due to the scrambler, and hence too complex to implement. A compromise can be found by performing symbol level Multi-Stage Wiener Filtering (MSWF), which is an iterative solution in which the complexity per iteration becomes comparable to twice that of the RAKE receiver. Since the MSWF works best when the input is white, better

¹⁷ $\rho(\mathbf{X}) = \max\{|\lambda|, \lambda \in \Lambda(\mathbf{X})\}$ where $\Lambda(\mathbf{X})$ is the eigenvalue matrix of \mathbf{X}

performance is obtained if the RAKE in each MSWF stage gets replaced by a chip equalizer-correlator. One of the main contributions here is to point out that the chip equalizer benefits from a separate optimization in every stage. This is shown through a mix of analysis and simulation results.

LMMSE receiver is complex for UMTS FDD mobile terminals since it not only requires inversion of a large user cross-correlation matrix but also needs the code and the amplitude knowledge of all the active users [24]. Furthermore, LMMSE solution changes every chip period due to aperiodic scrambling. The LMMSE *chip* equalizer-correlator is a suboptimal but much simpler alternative which is derived by modeling the scrambler as a stationary random sequence [20, 21]. Another suboptimal multiuser detector that *explicitly* focuses on subtracting the signals of interfering codes is the Parallel Interference Canceling (PIC) receiver [43]. It is well known that, under very relaxed cell loads, when the number of iterations goes to infinity, PIC might converge to the decorrelating receiver [22]. However, provided that it converges, still the convergence rate is very slow and it requires many stages to obtain a reasonable performance. This is due to the existence of high cross-correlations among users, which in fact is a consequence of the low orthogonality factor obtained initially from the use of Rake receiver in the front-end [7, 25, 29]. In this text, to at least guarantee the convergence in realistic loading factor situations and to increase the speed of convergence, we start the decorrelation operation, i.e., the zero forcing (ZF) *symbol* equalization from the output of LMMSE chip equalizer correlator front end receiver whose orthogonality factor is higher than the Rake receiver. For approximating this matrix inversion operation, we consider the polynomial expansion (PE) technique which is a better structured equivalent of PIC [26]. Until recently interference cancellation has been considered somewhat reluctantly for the downlink since it unrealistically requires knowing the locations of active codes in the OVSF tree and the amounts of powers they carry. Only recently the merits of intercell interference cancellation have been acknowledged [5] and efforts at finding viable solutions have been redoubled. The problem of OVSF code identification can be simplified by an equivalent modeling of the active multi-rate transmission system as a multi-code pseudo-transmission system at any chosen single SF-level L in the OVSF hierarchy. One toy example representing actually the UMTS-TDD case that contains SFs ranging from 1 to 16 is given in Fig. 21. In this example, the nodes corresponding to the active codes at SF-levels 4 and

8 are demonstrated by black bulbs. Their pseudo-equivalents at SF-level 16 (i.e., $L = 16$) are demonstrated by zig-zag pattern bulbs.

One can detect the existence or absence of pseudo-codes at the pseudo-level by comparing the powers at their correlator outputs with a noise-floor threshold [23]. These multiple correlations can be implemented with $O(L \log L)$ complexity by using Fast Walsh Hadamard Transformation (FWHT). Unitary FWHTs (U-FWHT) with proper dimensions can be logically/physically exploited to see/implement the two-way transformations between actual symbol sequences corresponding to the known codes (e.g., HSDPA codes) at various SF-levels and their pseudo-symbol sequence equivalents at a single SF-level. Fig. 22 demonstrates the two-way transformations between L_2/L_1 consecutive (time-multiplexed) actual symbols a_i at level L_1 and L_2/L_1 parallel (code-multiplexed) pseudo-symbols \tilde{a}_i at a larger SF-level L_2 . $P_{\{L_2/L_1\}}/S$ and $S/P_{\{L_2/L_1\}}$ are parallel to serial and serial to parallel converters from/to a bus size L_2/L_1 . When actual symbols reside at a higher SF-level, the two transformations have reverse roles.

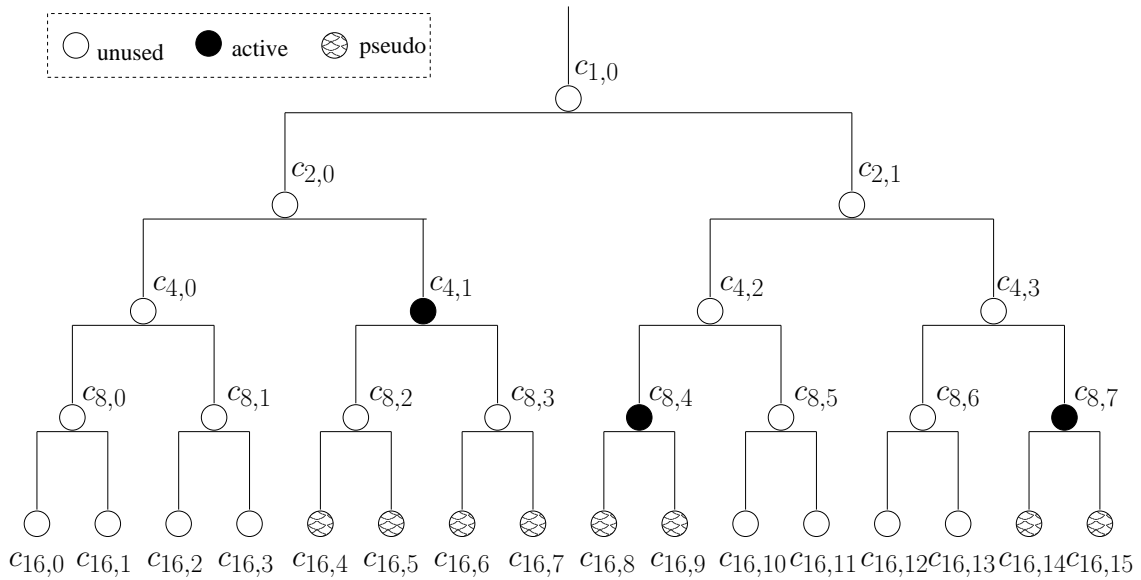


Figure 21: Equivalency of active-multirate and pseudo-multicode systems

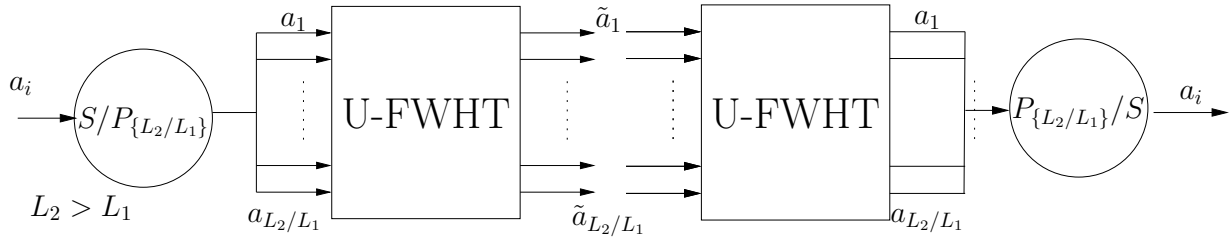


Figure 22: Transformations between actual and pseudo symbols

Polynomial Expansion Receiver

In this section, we develop parallel intracell interference canceling (IC) structures based on polynomial expansion (PE) technique which was initially proposed in [26]. We exploit the *pseudo-equivalency* concept at the highest *active* SF-level, SF-256, in the UMTS-FDD downlink for applying PE at this level. We ignore the existence of SF-512 since it is rarely used carrying control commands during an upload operation. The rationale for choosing the *highest active SF*, henceforth called L , is to obtain the highest possible degree of freedom in determining the PE subspace. If any other level L_x were selected, then an activity on a child code of $c_{x,i}$, $i \in \{0, \dots, L_x - 1\}$, say at a level $L_y > L_x$ on $c_{y,j}$, $j \in \{(L_y/L_x)i, \dots, (L_y/L_x)(i+1) - 1\}$, would render mandatory the implicit inclusion of also all the other child codes of $c_{x,i}$ at level L_y by including $c_{x,i}$ in the PE. This would have an adverse effect of noise amplification.

Pseudo-codes might be used in place of the *unknown actual codes* since the actual symbol estimates and their powers are not necessary as long as the pseudo-symbols are treated linearly in interference cancellation. However, knowing or detecting the actual codes is an opportunity for exploiting hard or hyperbolic-tangent nonlinearities or even channel decoding and encoding to refine their symbol estimates [10, 18]. In the latter case, one can pass between the symbol blocks of known codes and their pseudo-equivalents at SF-256 by properly dimensioned FWHTs. Through this hybrid treatment, i.e., respective nonlinear and linear treatment of known and unknown codes, becomes possible.

We model the discrete time received signal over one pseudo-symbol period as

$$\mathbf{Y}[n] = \mathbf{H}(z)\mathbf{S}[n]\mathbf{C}\mathbf{A}[n] + \mathbf{V}[n] = \tilde{\mathbf{G}}(n, z)\mathbf{A}[n] + \mathbf{V}[n]$$

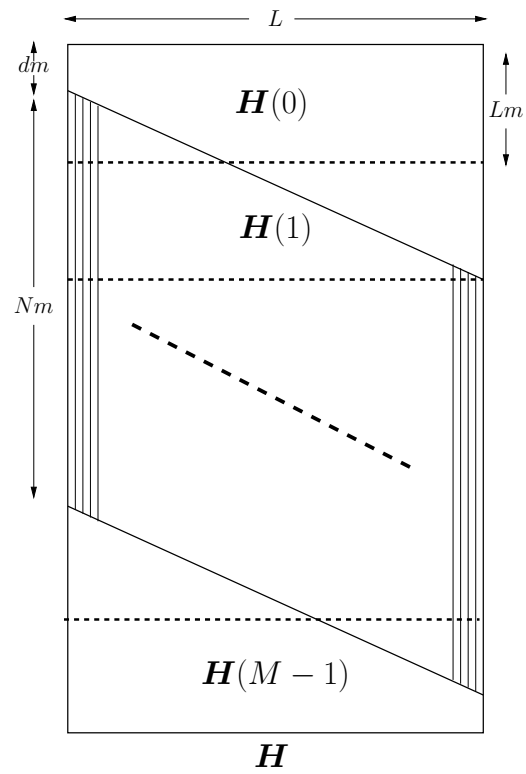


Figure 23: Channel impulse response of $H(z)$.

representing the system at the symbol rate. As shown in Figure 23, $\mathbf{H}(z) = \sum_{i=0}^{M-1} \mathbf{H}[i] z^{-i}$ is the symbol rate $Lm \times L$ channel transfer function, z^{-1} being the symbol period delay operator. The block coefficients $\mathbf{H}(i)$ are the $M = \lceil \frac{L+N+d-1}{L} \rceil$ parts of the block Toeplitz matrix with $m \times 1$ sized blocks, \mathbf{h} being the first column whose top entries might be zero for it comprises the transmission delay d between the BS and the mobile terminal. In this representation, $\mathbf{H}[0]$ carries the signal part corresponding to $\mathbf{A}[n]$ where there is no user of interest inter-symbol interference (ISI) but only user of interest inter-chip interference (ICI) and multi-user interference (MUI). $\mathbf{H}(i)$, ($i \in \{1, 2, \dots, M-1\}$), similarly, carries the ICI and MUI from $\mathbf{A}[n-i]$. The $L \times L$ matrix $\mathbf{S}[n]$ is diagonal and contains the scrambler for symbol period n . The column vector $\mathbf{A}[n]$ contains the K (pseudo-)symbols and \mathbf{C} is the $L \times K$ matrix of the K active codes.

Although it is possible to find an FIR left inverse filter for $\tilde{\mathbf{G}}(n, z)$ provided that $Lm \geq K$, this is not practical since $\tilde{\mathbf{G}}(n, z)$ is time-varying due to the aperiodicity of the scrambling. Therefore, we will introduce a less complex approximation to this inversion based on the polynomial expansion technique [26]. Instead of basing the receiver directly on the received signal, we shall first introduce a dimensionality reduction step from Lm to K by equalizing the channels with Linear Minimum Mean Square Error Zero Forcing (LMMSE-ZF) chip rate equalizers $\mathbf{F}(z)$ followed by a bank of correlators. LMMSE-ZF equalizer is the one among all possible ZF equalizers which minimizes the MSE at the output [14].

Let $\mathbf{X}[n]$ be the $K \times 1$ correlator output, which would correspond to the Rake receiver outputs if channel matched filters were used instead of channel equalizers. Then,

$$\begin{aligned} \mathbf{X}[n] &= \tilde{\mathbf{F}}(n, z) \mathbf{Y}[n] \\ &= \mathbf{C}^H \mathbf{S}^H [n] \mathbf{F}(z) (\tilde{\mathbf{G}}(n, z) \mathbf{A}[n] + \mathbf{V}[n]) \\ &= \mathbf{M}(n, z) \mathbf{A}[n] + \tilde{\mathbf{F}}(n, z) \mathbf{V}[n] \end{aligned}$$

where $\mathbf{M}(n, z) = \tilde{\mathbf{F}}(n, z) \tilde{\mathbf{G}}(n, z)$ and ZF equalization results in $\mathbf{F}(z) \mathbf{H}(z) = \mathbf{I}$. Hence,

$$\mathbf{M}(n, z) = \sum_{i=-\infty}^{\infty} \mathbf{M}[n, i] z^{-i} = \begin{bmatrix} \mathbf{I} & * \\ * & \mathbf{I} \end{bmatrix} \quad (54)$$

due to proper normalization of the code energies.

In order to obtain the estimate of $\mathbf{A}[n]$, we initially consider the processing of $\mathbf{X}[n]$ by a decorrelator as

$$\begin{aligned}\widehat{\mathbf{A}}[n] &= \mathbf{M}(n, z)^{-1} \mathbf{X}[n] \\ &= (\mathbf{I} - \overline{\mathbf{M}}(n, z))^{-1} \mathbf{X}[n].\end{aligned}\tag{55}$$

The correlation matrix $\mathbf{M}(n, z)$ has a coefficient $\mathbf{M}[n, 0]$ with a dominant unit diagonal in the sense that all other elements of the $\mathbf{M}[n, i]$ are much smaller than one in magnitude. Hence, the polynomial expansion approach suggests to develop $(\mathbf{I} - \overline{\mathbf{M}}(n, z))^{-1} = \sum_{i=0}^{\infty} \overline{\mathbf{M}}(n, z)^i$ up to some finite order, which leads to the iterative receiver as¹⁸

$$\begin{aligned}\widehat{\mathbf{A}}^{(-1)} &= 0 \ ; \ i \geq 0 . \\ \widehat{\mathbf{A}}^{(i)} &= \mathbf{X} + \overline{\mathbf{M}} \widehat{\mathbf{A}}^{(i-1)} , \\ &= \mathbf{X} + (\mathbf{I} - \mathbf{M}) \widehat{\mathbf{A}}^{(i-1)} , \\ &= \widehat{\mathbf{A}}^{(i-1)} + \tilde{\mathbf{F}}^i (\mathbf{Y} - \tilde{\mathbf{G}} \widehat{\mathbf{A}}^{(i-1)}) .\end{aligned}\tag{56}$$

The resultant iterative receiver architecture is given in Figure 24 where the numbers in paranthesis indicate the iteration indices. A practical receiver would be limited to a few orders, the quality of which depends on the degree of dominance of the static part of the diagonal of $\mathbf{M}(n, z)$ given in (56) with respect to the ICI carrying dynamic contents of the diagonal elements and multiuser interference (MUI) carrying off-diagonal elements.

In an iterative PE approach, it is advantageous to replace several *local* receiver components obtained from *global* LMMSE-ZF formulation by their LMMSE counterparts. Such modifications should lead to smaller offdiagonal power and hence faster convergence of the iterations to an estimate that is closer to a global MMSE estimate. For example LMMSE-ZF chip equalizers can be replaced by LMMSE equalizers which, though perturb the orthogonal structure of the received signal from the BS, do not enhance as much the intercell interference plus noise [28]. Furthermore some symbol feedback functionalities \mathcal{D} shown in Figure 25

¹⁸time indices are dropped for brevity

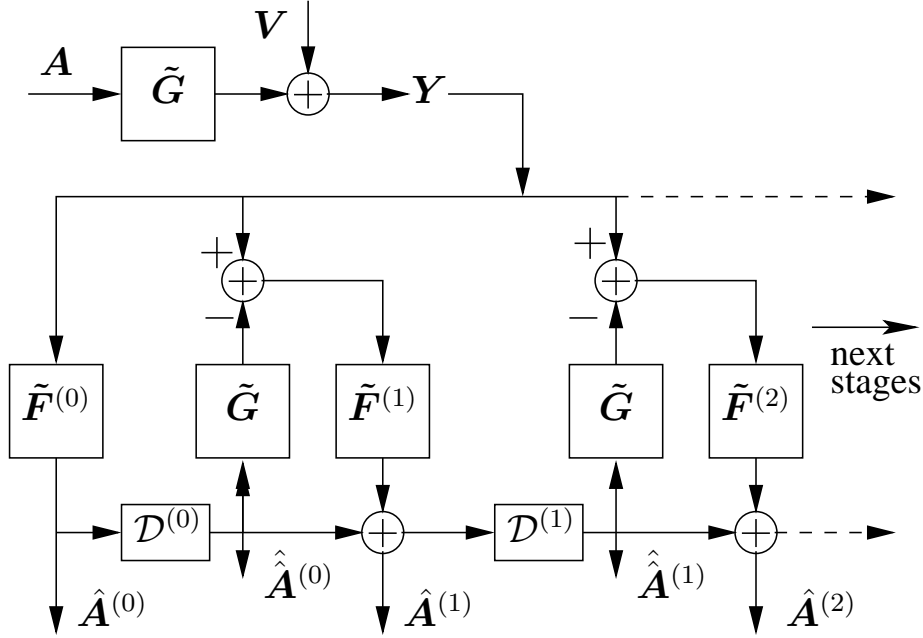


Figure 24: Polynomial expansion receiver

such as LMMSE weighting factors, hard decisions, a variety of soft decisions like hyperbolic-tangent functionality or even channel decoding and encoding blocks can be introduced.

Filter Adaptation

Figure 26 shows the open form of the receiver in Figure 24 where we clearly see the chip level blocks. In case the symbol feedback functionality \mathcal{D} is the identity matrix, we can further obtain a third equivalent architecture given in Figure 27 which, different from the previous two, iterates over the *chip* estimates at chip level filter outputs.

Since the projection operation $\mathbf{S}[n]\mathbf{C}\mathbf{C}^H\mathbf{S}^*[n]$ is not a chip level operation and is not convolutive it cannot be easily integrated into the filter optimization process. Nevertheless it has two nice properties: the diagonal part is the deterministic value $\mathcal{C}_l\mathbf{I}$ where \mathcal{C}_l is the effective cell loading factor and the expected value of the non-diagonal part is zero. By considering only the diagonal parts of the local projection operations, we reach to the Multi-stage Wiener (LMMSE) filter adaptation procedure given in the equations group (57) where $\{\boldsymbol{x}_i, \boldsymbol{y}_i, \tilde{\mathbf{B}}_i\}$ respectively denote {transfer function between the BS signal and the residual BS signal, transfer function for the intercell interference plus noise, the residual interference

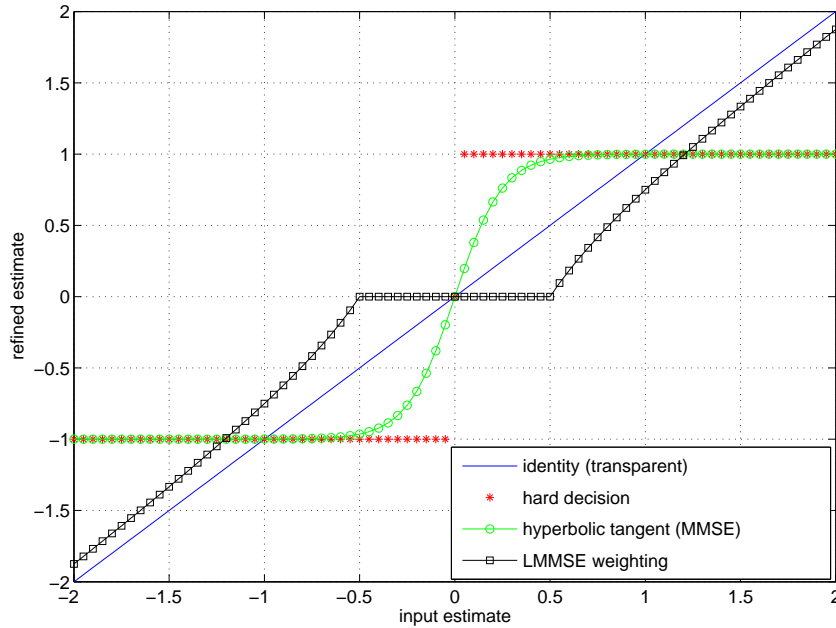


Figure 25: Feedback functionalities for real and imaginary parts of QPSK symbols which have 6 dB SINR

plus noise} at iteration i ¹⁹. The Wiener (LMMSE) filter and the unbiased LMMSE filter are denoted by \mathbf{F}_i^w and \mathbf{F}_i respectively.

The LMMSE optimization process output is the complete filter expression of \mathbf{F}_i from which we derive its two ingredients $\mathbf{S}_{\tilde{b}_{i-1}\mathbf{y}_i}$ and $\mathbf{S}_{\mathbf{y}_i\mathbf{y}_i}$ by *factorization*. The structure of the factorized terms are clear guidelines for understanding that, when unbiased, the chip level filter \mathbf{F}_i intends to estimate and subtract the *residual interference plus noise* term at the preceding iteration, which is expected to be also valid for systems with additional system components such as hard decisions. For example, if we consider the loop among the signals \hat{b}_0 , \mathbf{y}_1 and \hat{b}_1 that contains the transfer functions $\mathbf{F}_1(z)$ and $\mathbf{H}(z)$, it estimates the residual signal \tilde{b}_0 and subtracts it from \hat{b}_0 which leads to the creation of the new residual signal \tilde{b}_1 . The same reasoning holds for subsequent iterations where the amount of interference plus noise variance $\sigma_{\tilde{b}_i}^2$ is expected to decrease with increasing i as long as the spectral radius $\rho(\mathbf{I} - \mathbf{C}_i\mathbf{F}_i\mathbf{H}) < 1$.

¹⁹Each bold variable in Section 0.5.6 has a (z) suffix which is dropped for brevity; † stands for z-transform para-conjugate operator meaning matched filter in the time domain

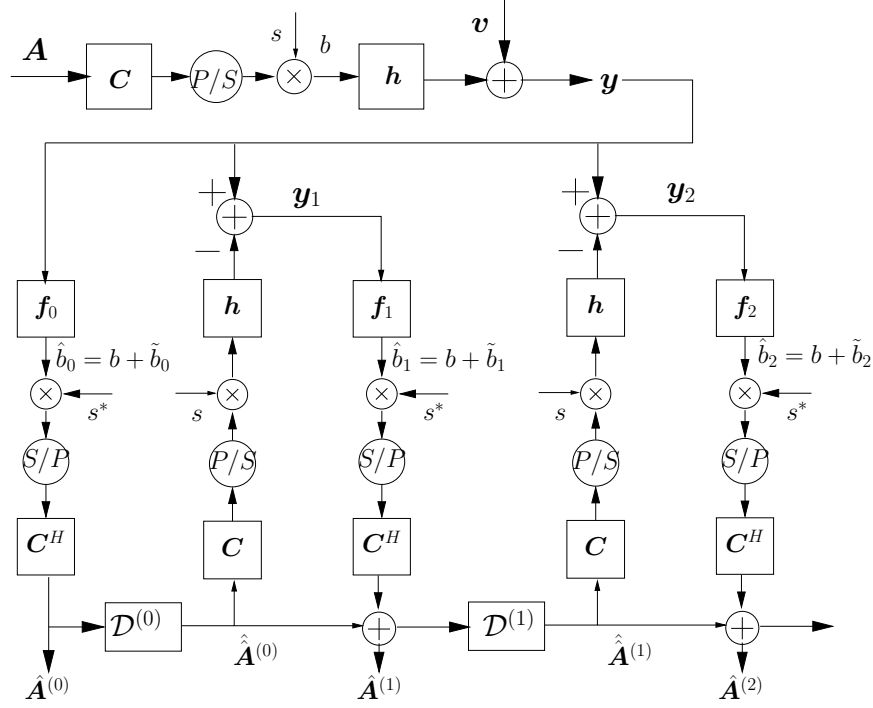


Figure 26: Polynomial expansion receiver open format.

INITIALIZATION (First Stage)

$$\mathcal{X}_0 = F_0 \mathbf{H} - \mathbf{I}$$

$$\mathcal{Y}_0 = F_0$$

$$\tilde{\mathbf{B}}_0 = \mathcal{X}_0 \mathbf{B} + \mathcal{Y}_0 \mathbf{V}$$

ITERATIONS (Interference Cancellation Stages)

for $(i > 0)$ and $(i < i_{max})$

$$\mathcal{X}_i = (\mathbf{I} - \mathcal{C}_l \mathbf{F}_i \mathbf{H}) \mathcal{X}_{i-1}$$

$$\mathcal{Y}_i = (\mathbf{I} - \mathcal{C}_l \mathbf{F}_i \mathbf{H}) \mathcal{Y}_{i-1} + \mathbf{F}_i$$

$$\tilde{\mathbf{B}}_i = \mathcal{X}_i \mathbf{B} + \mathcal{Y}_i \mathbf{V}$$

$$\arg_{\mathbf{F}_i^w} \min \frac{1}{2\pi j} \oint \frac{dz}{z} \left(\mathcal{X}_i \mathcal{X}_i^\dagger \sigma_b^2 + \mathcal{Y}_i \mathcal{Y}_i^\dagger \sigma_v^2 \right) \quad (57)$$

$$\mathbf{F}_i^w = \mathbf{S}_{\tilde{\mathbf{b}}_{i-1} \mathbf{y}_i} \mathbf{S}_{\mathbf{y}_i \mathbf{y}_i}^{-1}$$

$$\mathbf{S}_{\tilde{\mathbf{b}}_{i-1} \mathbf{y}_i} = \mathcal{C}_l \mathcal{X}_{i-1} \mathcal{X}_{i-1}^\dagger \mathbf{H}^\dagger \sigma_b^2 - \mathcal{Y}_{i-1} (\mathbf{I} - \mathcal{C}_l \mathbf{H} \mathcal{Y}_{i-1})^\dagger \sigma_v^2$$

$$\mathbf{S}_{\mathbf{y}_i \mathbf{y}_i} = \mathcal{C}_l^2 \mathbf{H} \mathcal{X}_{i-1} \mathcal{X}_{i-1}^\dagger \mathbf{H}^\dagger \sigma_b^2 + (\mathbf{I} - \mathcal{C}_l \mathbf{H} \mathcal{Y}_{i-1}) (\mathbf{I} - \mathcal{C}_l \mathbf{H} \mathcal{Y}_{i-1})^\dagger \sigma_v^2$$

$$\mathbf{F}_i = \frac{2\pi j \mathbf{F}_i^w}{\oint \frac{dz}{z} \mathbf{F}_i^w \mathbf{H}}: \text{unbiasing operation} \quad (58)$$

end

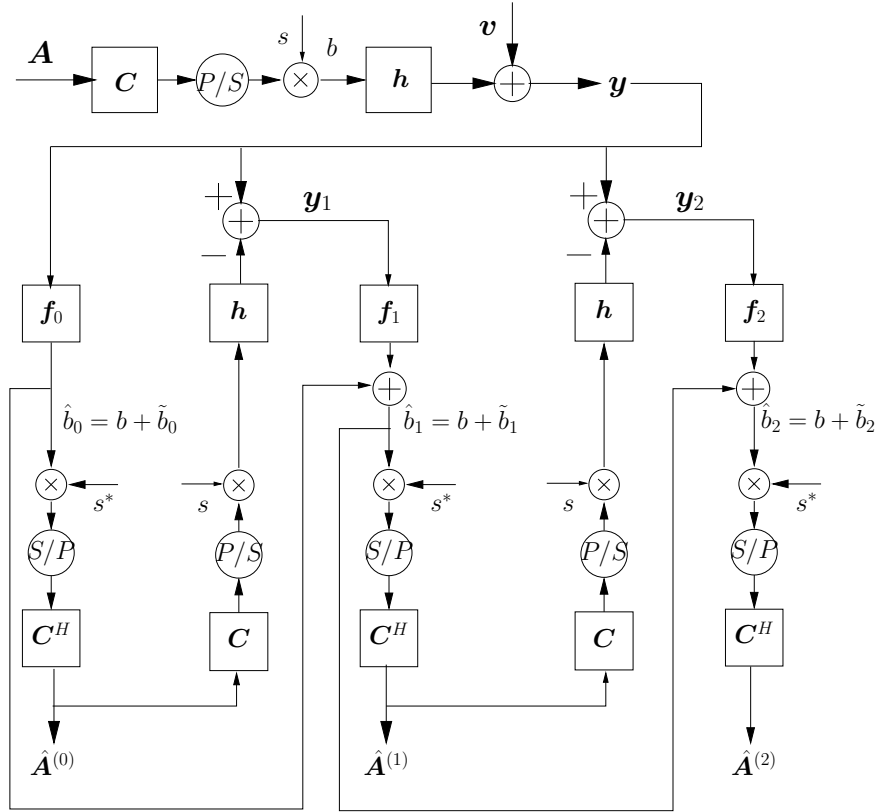


Figure 27: PE receiver equivalent chip estimate iterating model.

In practice, LMMSE chip equalizer correlator blocks might also be implemented as Generalized Rake (G-Rake) receivers in which case, in each stage, filtering with \mathbf{F}_i and \mathbf{H} will be similar to the filtering part of the Rake receiver [45]. Hence, each iteration will have twice the complexity of that of Rake.

Impact of Symbol Feedback Nonlinearities on Filter Expressions

When hard decisions or hyperbolic tangent nonlinearities are used on a subset of codes, we see two alternatives to reflect their impact to filtering expressions. The first approach is to simply assume that the associated symbols are perfectly estimated and hence to exclude them after first stage. In this case, the only required changes are to consider \mathcal{C}_l and σ_b^2 as respectively the loading factor and the sum chip variance of the remaining codes that are treated linearly. The second approach is to quantify the variances of the symbol estimation errors after the nonlinearities at every stage by the scheme and introduce new additive Gaussian noise sources at those points with the obtained variances.

Intercell Interference Cancellation Expansion

Polynomial expansion receiver can be modified to include also the intercell interference cancellation. The filter adaptations, the changes in signal modeling and the architecture for cancelling the interference of one neighboring BS are given in equations group (59), equations group (60) and Figure 28. The scheme can be easily extended to cover any number of cells by increasing the sizes of vectors and matrices in the equations group (60).

INITIALIZATION (First Stage)

$$\begin{aligned}\mathcal{X}_0 &= \mathbf{F}_0 \mathbf{H} - \mathbf{I} \\ \mathcal{Y}_0 &= \mathbf{F}_0 \\ \tilde{\mathbf{B}}_0 &= \mathcal{X}_0 \mathbf{B} + \mathcal{Y}_0 \mathbf{V}\end{aligned}$$

ITERATIONS (Interference Cancellation Stages)

for ($i > 0$) and ($i < i_{max}$)

$$\begin{aligned}\mathcal{X}_i &= (\mathbf{I} - \mathbf{F}_i \mathbf{H} \mathbf{C}_l) \mathcal{X}_{i-1} \\ \mathcal{Y}_i &= (\mathbf{I} - \mathbf{F}_i \mathbf{H} \mathbf{C}_l) \mathcal{Y}_{i-1} + \mathbf{F}_i \\ \tilde{\mathbf{B}}_i &= \mathcal{X}_i \mathbf{B} + \mathcal{Y}_i \mathbf{V} \\ \arg_{\mathbf{F}_{1,i}^w} \min & \frac{1}{2\pi j} \oint \frac{dz}{z} \left(\mathcal{X}_{1,i} \Sigma_b^2 \mathcal{X}_{1,i}^\dagger + \mathcal{Y}_{1,i} \mathcal{Y}_{1,i}^\dagger \sigma_v^2 \right) \\ \arg_{\mathbf{F}_{2,i}^w} \min & \frac{1}{2\pi j} \oint \frac{dz}{z} \left(\mathcal{X}_{2,i} \Sigma_b^2 \mathcal{X}_{2,i}^\dagger + \mathcal{Y}_{2,i} \mathcal{Y}_{2,i}^\dagger \sigma_v^2 \right) \\ \mathbf{F}_{1,i}^w &= \mathbf{S}_{\tilde{b}_{1,i-1} \mathbf{y}_i} \mathbf{S}_{\mathbf{y}_i \mathbf{y}_i}^{-1} \quad \mathbf{F}_{2,i}^w = \mathbf{S}_{\tilde{b}_{2,i-1} \mathbf{y}_i} \mathbf{S}_{\mathbf{y}_i \mathbf{y}_i}^{-1} \\ \mathbf{S}_{\tilde{b}_{1,i-1} \mathbf{y}_i} &= \mathbf{C}_{l_1} \mathcal{X}_{1,i-1} \Sigma_b^2 \mathcal{X}_{1,i-1}^\dagger \mathbf{H}_1^\dagger - \mathcal{Y}_{1,i-1} (\mathbf{I} - \mathbf{C}_{l_1} \mathbf{H}_1 \mathcal{Y}_{1,i-1})^\dagger \sigma_v^2 \\ \mathbf{S}_{\tilde{b}_{2,i-1} \mathbf{y}_i} &= \mathbf{C}_{l_2} \mathcal{X}_{2,i-1} \Sigma_b^2 \mathcal{X}_{2,i-1}^\dagger \mathbf{H}_2^\dagger - \mathcal{Y}_{2,i-1} (\mathbf{I} - \mathbf{C}_{l_2} \mathbf{H}_2 \mathcal{Y}_{2,i-1})^\dagger \sigma_v^2 \\ \mathbf{S}_{\mathbf{y}_i \mathbf{y}_i} &= \mathbf{H} \mathbf{C}_l \mathcal{X}_{i-1} \Sigma_b^2 \mathcal{X}_{i-1}^\dagger \mathbf{C}_l \mathbf{H}^\dagger + (\mathbf{I} - \mathbf{H} \mathbf{C}_l \mathcal{Y}_{i-1}) (\mathbf{I} - \mathbf{H} \mathbf{C}_l \mathcal{Y}_{i-1})^\dagger \sigma_v^2 \\ \mathbf{F}_{1,i} &= \frac{2\pi j \mathbf{F}_{1,i}^w}{\oint \frac{dz}{z} \mathbf{F}_{1,i}^w \mathbf{H}_1} \quad \mathbf{F}_{2,i} = \frac{2\pi j \mathbf{F}_{2,i}^w}{\oint \frac{dz}{z} \mathbf{F}_{2,i}^w \mathbf{H}_2}\end{aligned} \tag{59}$$

end

$$\begin{aligned}
\mathbf{A}[n] &\longrightarrow \begin{bmatrix} \mathbf{A}_1[n] \\ \mathbf{A}_2[n] \end{bmatrix} : \text{vector of symbols} \\
\mathbf{C} &\longrightarrow \begin{bmatrix} \mathbf{C}_1 & \mathbf{0} \\ \mathbf{0} & \mathbf{C}_2 \end{bmatrix} : \text{channelization codes} \\
\mathbf{S}[n] &\longrightarrow \begin{bmatrix} \mathbf{S}_1[n] & \mathbf{0} \\ \mathbf{0} & \mathbf{S}_2[n] \end{bmatrix} : \text{scrambling} \\
\mathbf{B} &\longrightarrow \begin{bmatrix} \mathbf{B}_1 \\ \mathbf{B}_2 \end{bmatrix} : \text{transmitted chip sequences} \\
\sigma_b^2 &\longrightarrow \Sigma_b^2 = \begin{bmatrix} \sigma_{b_1}^2 & 0 \\ 0 & \sigma_{b_2}^2 \end{bmatrix} : \text{chip level signal covariance} \\
\mathbf{H}(z) &\longrightarrow \begin{bmatrix} \mathbf{H}_1(z) & \mathbf{H}_2(z) \end{bmatrix} : \text{chip rate channel} \\
\mathbf{F}_i(z) &\longrightarrow \begin{bmatrix} \mathbf{F}_{1,i}(z) \\ \mathbf{F}_{2,i}(z) \end{bmatrix} : \text{chip level equalizers at iteration } i \\
\tilde{\mathbf{G}}(n, z) &\longrightarrow \begin{bmatrix} \tilde{\mathbf{G}}_1(n, z) & \tilde{\mathbf{G}}_2(n, z) \end{bmatrix} = \begin{bmatrix} \mathbf{H}_1(z)\mathbf{S}_1[n]\mathbf{C}_1 & \mathbf{H}_2(z)\mathbf{S}_2[n]\mathbf{C}_2 \end{bmatrix} : \text{symbol rate channel} \\
\tilde{\mathbf{F}}^{(i)}(n, z) &\longrightarrow \begin{bmatrix} \tilde{\mathbf{F}}_1^{(i)}(n, z) \\ \tilde{\mathbf{F}}_2^{(i)}(n, z) \end{bmatrix} : \text{symbol level equalizers at iteration } i \\
\boldsymbol{\chi}_i &\longrightarrow \begin{bmatrix} \boldsymbol{\chi}_{1,1,i} & \boldsymbol{\chi}_{1,2,i} \\ \boldsymbol{\chi}_{2,1,i} & \boldsymbol{\chi}_{2,2,i} \end{bmatrix} : \text{interference transfer function} \\
\boldsymbol{\chi}_{1,i} &= \begin{bmatrix} \boldsymbol{\chi}_{1,1,i} & \boldsymbol{\chi}_{1,2,i} \end{bmatrix} : \text{interference transfer function for the first BS signal} \\
\boldsymbol{\chi}_{2,i} &= \begin{bmatrix} \boldsymbol{\chi}_{2,1,i} & \boldsymbol{\chi}_{2,2,i} \end{bmatrix} : \text{interference transfer function for the second BS signal} \\
\boldsymbol{\gamma}_i &\longrightarrow \begin{bmatrix} \boldsymbol{\gamma}_{1,i} \\ \boldsymbol{\gamma}_{2,i} \end{bmatrix} : \text{noise transfer function} \\
\mathcal{C}_l &\longrightarrow \mathcal{C}_l = \begin{bmatrix} \mathcal{C}_{l_1} & 0 \\ 0 & \mathcal{C}_{l_2} \end{bmatrix} : \text{loading factors} \\
\mathbf{Y}[n] &\longrightarrow \begin{bmatrix} \mathbf{H}_1(z)\mathbf{S}_1[n]\mathbf{C}_1 & \mathbf{H}_2(z)\mathbf{S}_2[n]\mathbf{C}_2 \end{bmatrix} \begin{bmatrix} \mathbf{A}_1[n] \\ \mathbf{A}_2[n] \end{bmatrix} + \mathbf{V}[n] = \tilde{\mathbf{G}}(n, z) \mathbf{A}[n] + \mathbf{V}[n]
\end{aligned} \tag{60}$$

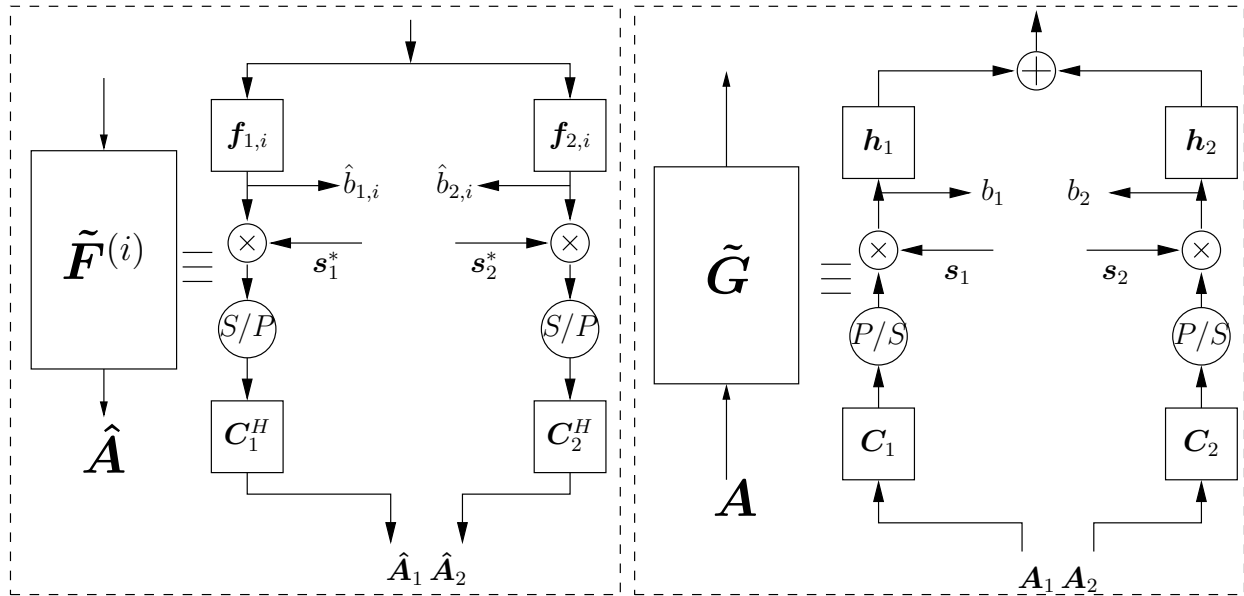


Figure 28: Symbol level transfer function blocks and their chip level equivalents

Simulations and Conclusions

For the simulations we consider only intracell interference cancellation.

We take a high speed downlink packet access (HSDPA) scenario in the UMTS-FDD downlink [5]. We consider 5 HSDPA codes at SF-16 assigned to the UE each consuming 8% of the base station power. The PCPICH pilot tone at SF-256 consumes 10% power. There is the PCCPCH code at SF-256 that consumes 4% power. To effectively model all the rest multirate user codes that we do not know, we place 46 pseudo-codes at level 256 each having 1% power. So in total, 5 HSDSCH codes at SF-16 being equivalent to 80 pseudo-codes at SF-256, the system is effectively 50% loaded with 128 (pseudo-)codes at SF-256, i.e., $C_l = 0.5$. Although, in practice, the pseudo-codes should be detected by a method explained in the text, for the moment, we assume that they are known. We also assume perfect knowledge of the channel. An oversampling factor of 2 and one receive antenna is used ²⁰. Static propagation channel parameters are randomly generated from the ITU Vehicular-A power

²⁰The order of filtering and rechanneling operations have an impact on the noise term in case of polyphase filtering which we neglect for the moment

delay profile. Pulse shape is the UMTS-standard, root-raised cosine with a roll-off factor of 0.22. Therefore the propagation channel, pulse shape cascade (i.e., the overall channel) has a length of 19 chips at 3.84 Mchips/sec transmission rate. Symbols are QPSK. \hat{I}_{or}/I_{oc} denotes the received base station power to intercell interference plus noise power ratio. We took the average SINR result of 5 HSDPA codes over 100 realizations of one UMTS slot (160 symbol period) transmissions.

Figure 29 shows the performances of the PE scheme with various different chip level filter usages and iterations from one to three. The legends indicate the used filters with iteration order. For example F0-F1-F2 means optimized filters are used in all the stages; F0-Rake-Rake hybrid scheme means first stage filter is LMMSE chip equalizer and subsequent two are Rake receivers; Rake-Rake-Rake corresponds to the *conventional* linear PIC. Many other variants different from the shown ones can also be used. As is expected Rake receiver performs the worst. The conventional Linear PIC with only Rake receivers starts diverging after first iteration especially in the I_{or}/I_{oc} values below 10dB. This is consistent with the literature since it is well known that, for guaranteeing the converge of the LPIC, loading factor should be lower than %17 [15]²¹. The scheme which uses only F0 does not improve significantly after second iteration. Using Rake receivers after F0 performs very well. As expected adapting the filters at all iterations performs the best. Such a scheme obtains almost the same performance of F0-Rake-Rake in one less iteration, i.e., with configuration F0-F1. At low \hat{I}_{or}/I_{oc} values which reflect the cell edge situations, the performance of the first iteration is better than the second one. This is due to the fact that at low SNR regions the gain from the interference reduction is not sufficient to compensate the loss from noise amplification, since the iterative scheme is still a decorrelation. One might also attribute this to the well-known *ping-pong* effect for LPIC [33].

Figure 30 shows the performances when we apply hard decisions on the 5 HSDPA codes which have an effective loading impact $\mathcal{C}_{HSDPA} = \frac{5}{16}$. With the assumption of correct decisions we subtract \mathcal{C}_{HSDPA} from the overall cell load of 0.5 and apply the $\mathcal{C}_l = \frac{3}{16}$ value in the filter adaptation process in (58). In this case using Rake receivers after first stage equalization catches up with the optimized filters after three stages. We also observe that

²¹in the random CDMA, flat fading case

conventional PIC also starts getting into a convergence trend. It is not however explicit from the \mathcal{X}_i and \mathcal{Y}_i expressions why things should improve despite the fact that the \mathcal{C}_i value decreases resulting in lower iteration gain in chip estimation. Due to this fact one would at first sight expect an inability of the interference reduction to compensate the amplified noise. This is however not the case due to the fact that almost all of the ingredients of the additional noise term coming from the previous iteration is in the subspace belonging to the codes whose symbols are estimated linearly whereas the final SINR performance metric is computed on codes such as HSDPA codes which are treated by hard decisions. In the full linear treatment however, the additional noise that traverses the iterations with amplification is in the whole signal space. Therefore when hard decisions are applied there is an implicit reduction of additional noise by a factor $\frac{\mathcal{C}_i}{\mathcal{C}_i + \mathcal{C}_{HSDPA}}$. These interpretations seem to be conflicting with the chip equalizer adaptation expressions where we ignored the non-diagonal part of the projection operation $\mathbf{S}[n]\mathbf{C}\mathbf{C}^H\mathbf{S}^*[n]$ in order to recover from the dependence on codes. For the interpretations of performances at symbol levels however one has to look from a different perspective, taking into account the code knowledge.

Comparing Figure 29 and Figure 30 we observe that at medium and high \hat{I}_{or}/I_{oc} working regions hard decisions increase the obtained SINR by 1 to 3 dB. At low \hat{I}_{or}/I_{oc} regions there is no gain, which is understandable since in those regions hard decisions are not reliable.

We next look at the orthogonality factor histograms of the considered receivers by randomly generating 10^4 static channels from the Vehicular A power delay profile with and \hat{I}_{or}/I_{oc} value of 10dB. Figure 31 shows the histograms for the CMF and LMMSE equalizer. We see that, besides giving worse median OF, CMF might also give OFs less than 0.4. In Figure 32, Figure 33 and Figure 34 we respectively see the trend of OFs obtained from all CMF usage, CMF usage after first stage equalization and all chip level LMMSE equalizer usage in LPIC iterations. In order to obtain them, we first compute the $\|\mathbf{x}_i\|^2$ and pass to OF as $\alpha_i = \frac{1}{1 + \|\mathbf{x}_i\|^2}$ since all the filters are unbiased. The histograms in Figure 32 clearly demonstrate the problem with conventional LPIC. From median value perspective the OF first improves at first stage and then starts degrading. Even more important concern is the widening of OF range. After four iterations there are even channel cases where OF is close to zero. The histograms in Figure 33 demonstrate the importance of LMMSE chip equalization

as a starting point. Although there are still a very little amount of corner cases leading to small OFs, the overall performance is at an acceptable level. Finally the histograms in Figure 33 clearly indicate the strength of using optimized chip equalizers at all stages. Not only the median value but also the worst case OF improves with every iteration. 0.86 at first and fourth stages respectively. In brief we can say that when the mobile knows multiple codes as in the HSDPA service, applying Rake receivers after a first stage equalization stage is a proper choice. In the case of only one code however it is beneficial to adapt filters at every stage.

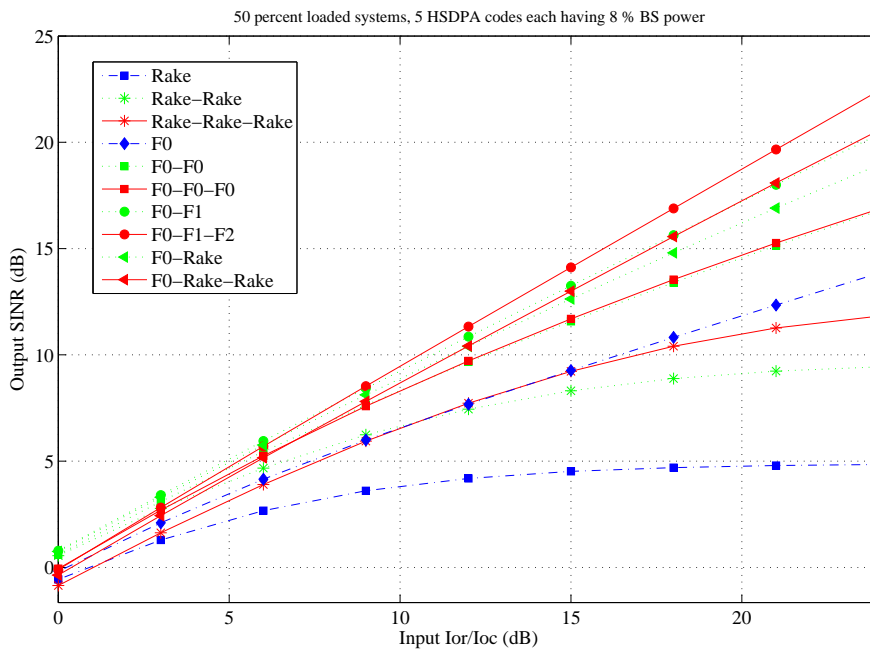


Figure 29: SINR vs \hat{I}_{or}/I_{oc} linear decisions results, Vehicular A channel, N=19

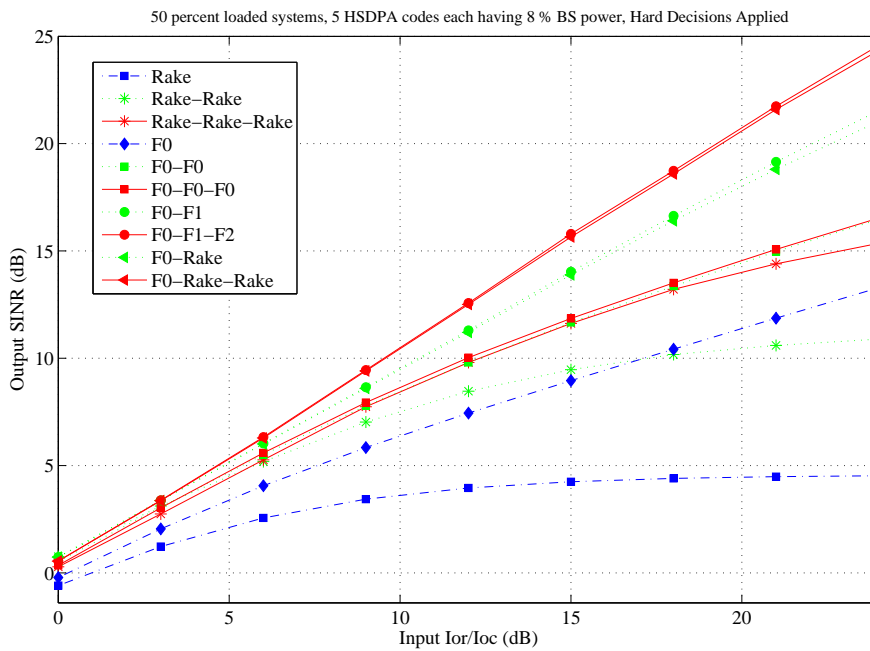


Figure 30: SINR vs \hat{I}_{or}/I_{oc} hard decisions results, Vehicular A channel, N=19

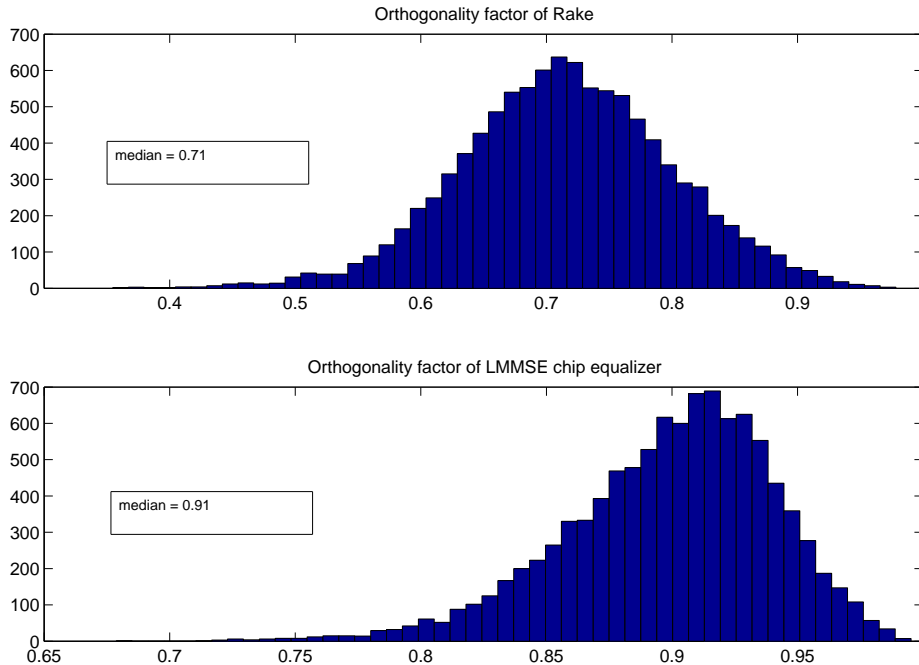


Figure 31: Orthogonality factor histograms of 2-phase CMF and 2-phase LMMSE chip equalizer in Vehicular A channel with $\hat{I}_{or}/I_{oc} = 10dB$

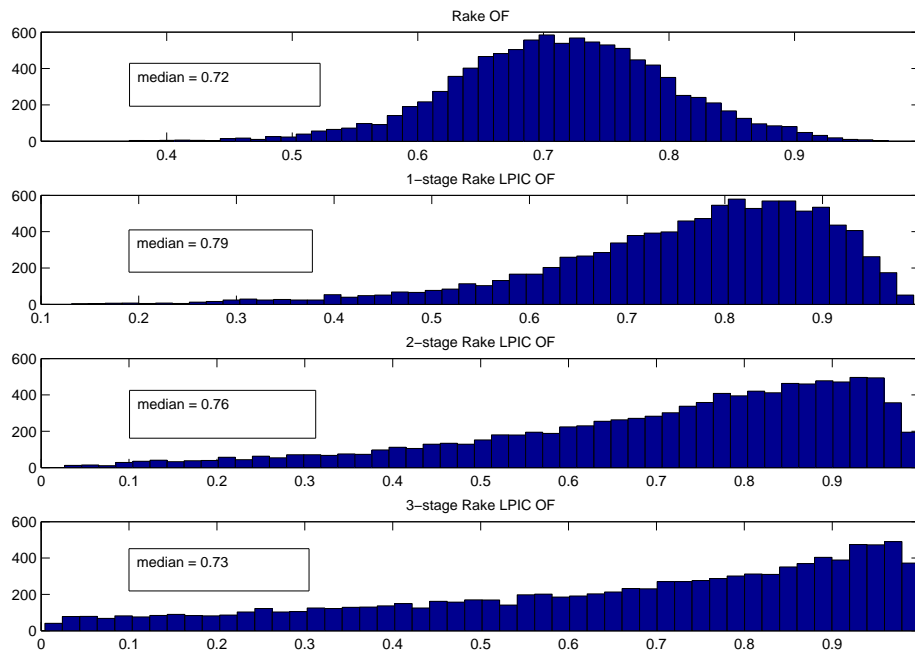


Figure 32: Orthogonality factor histogram of conventional LPIC with 2-phase CMF in the Vehicular A channel

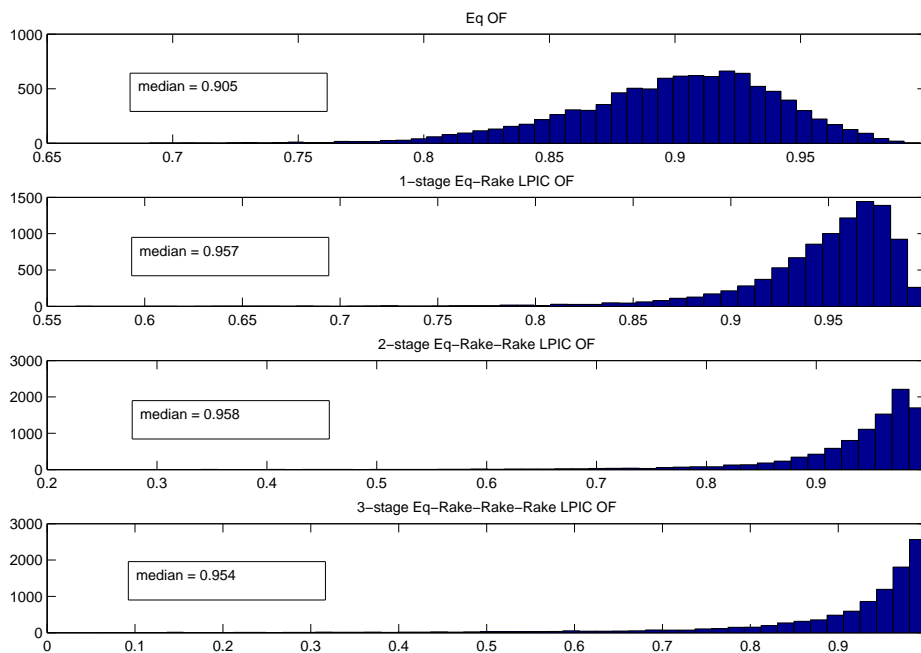


Figure 33: Orthogonality factor histogram of LPIC with first stage 2-phase LMMSE chip equalizer followed by 2-phase CMFs in the Vehicular A channel with $\hat{I}_{or}/I_{oc} = 10dB$

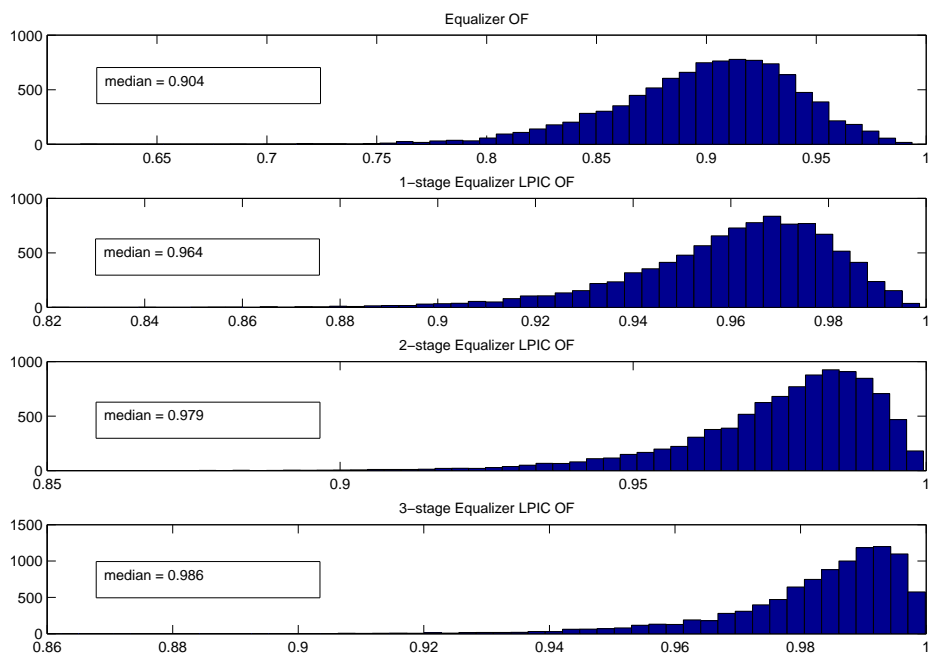


Figure 34: Orthogonality factor histogram of LPIC with 2-phase LMMSE chip equalizers in all stages in the Vehicular A channel with $\hat{I}_{or}/I_{oc} = 10dB$

References

- [1] Physical layer aspects of HSDPA. Technical Report TS 25.848, 3GPP, [Online]. Available: <http://www.3gpp.org/ftp/Specs>.
- [2] Physical layer procedures (FDD). Technical Report TS 25.214, 3GPP, [Online]. Available: <http://www.3gpp.org/ftp/Specs>.
- [3] QoS concept and architecture. Technical Report TS 23.107, 3GPP, [Online]. Available: <http://www.3gpp.org/ftp/Specs>.
- [4] Technical specifications. Technical report, 3GPP, [Online]. Available: <http://www.3gpp.org>.
- [5] User equipment (UE) radio transmission and reception (FDD) - release 8. Technical Report TS 25.101, 3GPP, [Online]. Available: <http://www.3gpp.org/ftp/Specs>.
- [6] UTRA high speed downlink packet access; overall UTRAN description. Technical Report TS25.855, 3GPP, [Online]. Available: <http://www.3gpp.org/ftp/Specs>.
- [7] R. Michael Buehrer, S. P. Nicoloso, and S. Gollamudi. Linear versus nonlinear interference cancellation. *Journal of Communications and Networks*, 1, June 1999.
- [8] C. Cozzo, G. E. Bottomley, and A. S. Khayrallah. Rake receiver finger placement for realistic channels. In *Proc. of the Wireless Communications and Networking Conference*, pages 316–321, 2004.
- [9] H. P. Decell. An application of the Cayley-Hamilton theorem to generalized matrix inversion. *Jr. SIAM Review*, 7, No.4:526–528, October 1965.
- [10] D. Divsalar, M.K. Simon, and D. Raphaeli. Improved parallel interference cancellation. *IEEE Transactions on Communications Theory*, 46:258–268, February 1998.
- [11] A. Duel-Hallen. Decorrelating decision-feedback multiuser detector for synchronous code-division multiple-access channel. *IEEE Transactions on Communications*, 41(2):285–290, February 1993.
- [12] P. Frenger, S. Parkvall, and E. Dahlman. The evolution of WCDMA towards higher speed downlink packet data access. In *Proc. of the Vehicular Technology Conf.*, October 2001.
- [13] Irfan Ghauri and Dirk T. M. Slock. Linear receivers for the DS-CDMA downlink exploiting orthogonality of spreading sequences. In *Proc. 32nd Asilomar Conf. on Signals, Systems & Computers*, volume 1, pages 650–654, Pacific Grove, CA, November 1998.
- [14] Irfan Ghauri and Dirk T. M. Slock. MMSE-ZF receiver and blind adaptation for multirate CDMA. In *Proc. Vehicular Technology Conf.*, September 1999.
- [15] A. Grant and C. Schlegel. Convergence of linear interference cancellation multiuser receivers. *IEEE Transaction on Communications*, 49(10), October 2001.
- [16] L.J. Greenstein, Y.S. Yeh, V. Erceg, and M. V. Clark. A new path gain/delay-spread propagation model for digital cellular channels. *IEEE Transactions on Vehicular Technology*, 46, no.2, May 1997.
- [17] H. Holma and A. Toskala. *WCDMA for UMTS*. John Wiley and Sons, 2000.
- [18] R. Irmer, A. Nahler, and G. Fettweis. On the impact of soft decision functions on the performance of multistage parallel interference cancelers for CDMA systems. In *Proc. Vehicular Tech. Conf.*, Rhodes, Greece, May 2001.
- [19] J. F. Kurose and K. W. Rose. *Computer Networking: A top down approach featuring the Internet*. Addison-Wesley, 2003.
- [20] M. Lenardi and D. T. M. Slock. SINR maximizing equalizer receiver for DS-CDMA. In *Proc. of the EUSIPCO Conf.*, Tampere, Finland, September 2000.
- [21] Massimiliano Lenardi and Dirk T. M. Slock. A RAKE structured SINR maximizing mobile receiver for the WCDMA downlink. In *Proc. of the Asilomar Conf. on Signals, Systems and Computers*, Pacific Grove, California, USA, November 2001.
- [22] R. Lupas and S. Verdú. Linear multiuser detectors for synchronous code-division multiple-access channels. *IEEE Transactions on Information Theory*, IT-35:123–136,

- January 1989.
- [23] M.F. Madcour, S.C. Gupta, and Y.E. Wang. Successive interference cancellation algorithms for downlink W-CDMA communications. *IEEE Transactions on Wireless Communications*, 1(1), January 2002.
 - [24] U. Madhow and M.L. Honig. MMSE interference suppression for direct-sequence spread-spectrum CDMA. *IEEE Trans. on Communications Theory*, 42:3178–3188, December 1994.
 - [25] N.B. Mehta, L.J. Greenstein, T.M. Willis, and Z. Kotic. Analysis and results for the orthogonality factor in WCDMA downlinks. In *Proc. of the Vehicular Technology Conf.*, May 2002.
 - [26] S. Moshavi, E. Kanterakis, and D. L. Schilling. Multistage linear receivers for DS-CDMA systems. *International Journal of Wireless Information Networks*, 3,No.1, 1996.
 - [27] R. R. Muller and S. Verdú. Design and analysis of low complexity interference mitigation on vector channels. *IEEE Journal on Selected Areas in Communications*, 19(8):1429–1441, August 2001.
 - [28] C. Papadias and D.T.M. Slock. Fractionally spaced equalization of linear polyphase channels and related blind techniques based on multichannel linear prediction. *IEEE Transactions on Signal Processing*, 47, no.3, March 1999.
 - [29] K.I. Pedersen and P.E. Mogensen. The downlink orthogonality factors influence on WCDMA system performance. In *Proc. of the Vehicular Technology Conf.*, September 2002.
 - [30] H. Poor and S. Verdú. Probability of error in MMSE multiuser detection. *IEEE Transactions on Information Theory*, 43, no.3, May 1997.
 - [31] J. G. Proakis. *Digital Communications*. NY: McGraw-Hill, 3rd edition, 1995.
 - [32] T. S. Rappaport. *Wireless Communications - Principles and Practice*. Prentice Hall, Upper Saddle River, NJ, 1996.
 - [33] L. K. Rasmussen and I. J. Oppermann. Ping-pong effects in linear parallel interference cancellation for CDMA. *IEEE Trans. on Wireless Comm.*, 2(2):357–363, March 2003.
 - [34] COST231 Final Report. Digital mobile radio towards future generation systems. Technical report, COST Telecom Secretariat, European Commission, Brussels, Belgium, 1999.
 - [35] J.S. Sadowsky, D. Yellin, S. Moshavi, and Y. Perets. Cancellation accuracy in CDMA pilot interference cancellation. In *Proc. of the Vehicular Technology Conf.*, April 2003.
 - [36] J.S. Sadowsky, D. Yellin, S. Moshavi, and Y. Perets. Capacity gains from pilot cancellation in CDMA networks. In *Proc. of the Wireless Communications and Networking Conf.*, March 2003.
 - [37] C. Schlegel, S. Roy, P. Alexander, and Z. Xiang. Multiuser projection receivers. *IEEE J. on Selected Areas in Communications*, 14(8):1610–1618, October 1996.
 - [38] Dirk T.M. Slock and Irfan Ghauri. A blind maximum SINR receiver for the DS-CDMA forward link. In *Proc. ICASSP'2000*, Istanbul, Turkey, June 2000.
 - [39] W. Stallings. *Data and Computer Communications, Seventh Edition*. Prentice Hall, 7 edition, May 2003.
 - [40] G. Strang. *Introduction to Linear Algebra*. Wellesley-Cambridge Press, third edition, June 1998.
 - [41] TIA/EIA/IS-95. Mobile Station Base-Station Compatibility Standard for Dual-Mode Wideband Spread Spectrum Cellular System. Technical report, Telecommunication Industry Association, 1993.
 - [42] D. Tse and P. Viswanath. *Fundamentals of Wireless Communication*. Cambridge University Press, May 2005.
 - [43] M.K. Varanasi and B. Aazhang. Multistage detection in asynchronous code-division multiple-access communications. *IEEE Transactions on Communications Theory*, 38:509–519, Apr 1990.

- [44] S. Verdú. *Multiuser Detection*. Cambridge University Press, 1998.
- [45] Y. P.E. Wang and G. E. Bottomley. Generalized Rake reception for cancelling interference from multiple base stations. In *Proc. Vehicular Tech. Conf.*, Boston, Massachusetts - USA, September 2000.
- [46] K. Zayana and B. Guisnet. Measurements and modelisation of shadowing cross-correlations between two base stations. In *Proc. of the ICUPC*, Rome, Italy, October 1998.
- [47] J. Zhang, E.K.P. Chong, and D.N.C. Tse. Output MAI distributions of linear MMSE multiuser receivers in DS-CDMA systems. *IEEE Transactions on Information Theory*, 47, no.3, March 2001.